HHS Public Access

Author manuscript

Chem Soc Rev. Author manuscript; available in PMC 2016 March 02.

Published in final edited form as:

Chem Soc Rev. 2011 July ; 40(7): 3677–3702. doi:10.1039/c0cs00138d.

Flexible fabrication and applications of polymer nanochannels and nanoslits

Rattikan Chantiwas[†,a], **Sunggook Park**[a], **Steven A. Soper**[a], **Byoung Choul Kim**[b], **Shuichi Takayama**[b], **Vijaya Sunkara**[c], **Hyundoo Hwang**[c], and **Yoon-Kyoung Cho**[c]

[a] Department of Chemistry and Department of Mechanical Engineering, Louisiana State University, Baton Rouge, LA, 70803, USA

[b] Department of Biomedical Engineering, University of Michigan, Ann Arbor, MI, 48109, USA

[c]School of Nano-Bioscience and Chemical Engineering, Ulsan National Institute of Science and Technology, Ulsan, 689-798, Korea

Abstract

Fluidic devices that employ nanoscale structures (<100 nm in one or two dimensions, slits or channels, respectively) are generating great interest due to the unique properties afforded by this size domain compared to their micro-scale counterparts. Examples of interesting nanoscale phenomena include the ability to preconcentrate ionic species at extremely high levels due to ion selective migration, unique molecular separation modalities, confined environments to allow biopolymer stretching and elongation and solid-phase bioreactions that are not constrained by mass transport artifacts. Indeed, many examples in the literature have demonstrated these unique opportunities, although predominately using glass, fused silica or silicon as the substrate material. Polymer microfluidics has established itself as an alternative to glass, fused silica, or silicon-based fluidic devices. The primary advantages arising from the use of polymers are the diverse fabrication protocols that can be used to produce the desired structures, the extensive array of physiochemical properties associated with different polymeric materials, and the simple and robust modification strategies that can be employed to alter the substrate's surface chemistry. However, while the strengths of polymer microfluidics is currently being realized, the evolution of polymer-based nanofluidics has only recently been reported. In this *critical review*, the opportunities afforded by polymer-based nanofluidics will be discussed using both elastomeric and thermoplastic materials. In particular, various fabrication modalities will be discussed along with the nanometre size domains that they can achieve for both elastomer and thermoplastic materials. Different polymer substrates that can be used for nanofluidics will be presented along with comparisons to inorganic nanodevices and the consequences of material differences on the fabrication and operation of nanofluidic devices (257 references).

Correspondence to: Sunggook Park; Steven A. Soper; Shuichi Takayama; Yoon-Kyoung Cho.

[†]Current address: Department of Chemistry and Center of Excellence for Innovation in Chemistry, Faculty of Science, Mahidol University Rama 6 Road, Bangkok 10400, Thailand.

1. Introduction

There have been a number of reviews focused on the fabrication of nanoslits (nanoslits are defined here as conduits that have one dimension below 100 nm) and/or nanochannels (nanochannels are defined as conduits with two dimensions below 100 nm) and their applications resulting primarily from unique phenomena that occur in nano-confined environments but do not exist in micro-scale environments.[1–4] Indeed, a recent issue appearing in *Chemical Society Reviews* (2010, Vol. 39, Issue 3) dealt specifically with reviewing basic phenomena unique to nano-confined environments, such as ion transport,[5] nanofluidic diodes,[6] concentration polarization,[7,8] capillarity[9] and voltage responsive structures.[10] In addition, many applications of nanofluidic systems were reviewed such as DNA manipulations and mapping,[11,12] tether forces in DNA electrophoresis[13] and chemical analyses.[14,15] In many of these applications, phenomena that occur in nano-confined environments are necessary to realize the intended goal of the application. For example, in micro-scale environments, double-stranded DNA (dsDNA) exists as a randomly coiled structure whereas in nanoenvironments, the dsDNA will stretch to near its full contour length allowing the ability to either size the dsDNA molecule directly or observe enzymatic cutting of the DNA to identify certain sequence locations, such as restriction sites.[16] In terms of DNA sequencing, translocation of single-stranded DNA through nanochannels with dimensions below its persistence length will provide an effective means to read the primary structure of DNAs directly using an electrical readout modality.[17]

The major focus of most reviews as well as the predominate literature dealing with nanofluidics has been directed toward devices that use glass, fused silica or silicon (Si) as the substrate material due to their established surface chemistry, excellent optical properties, and well-entrenched fabrication technologies. In addition, these brittle materials (*i.e.*, high Young's modulus) tend to maintain their form factors during thermal and/or pressure processing used for assembling devices to enclose the fluidic structures. Fabricating nanofluidic structures in these materials typically requires a lithography step in which a resist is patterned with nanofeatures using an electron beam (electron beam lithography, EBL) or nanoimprint lithography (NIL) followed by wet/dry etching or direct writing into the substrate using a focused ion beam (FIB). The shortcoming of these nanofabrication strategies is that they require extensive device processing steps, therefore making it difficult to realize the generation of low-cost devices conducive to mass production. The replication of these devices could potentially expand the user-base in performing nanofluidic experiments or transitioning this exciting technology into important application areas, such as *in vitro* diagnostics.

Polymers provide an attractive alternative to glass-based materials for nanofluidics due to their diverse range of physiochemical properties (see Section 1.1), low material cost, a variety of surface modification protocols that can be used (see Section 1.2) and a number of fabrication techniques that can be employed to make the prerequisite structures (see Sections 2 and 3). The fabrication modalities include such techniques as hot embossing, which have been well demonstrated in the area of microfluidics that can produce devices in a high production mode and at low-cost.[18,19]

In this *critical review*, we will provide an overview of the emerging area of polymer-based nanofluidics using both elastomeric and thermoplastic polymers. We will cover different fabrication techniques that can be used to produce nanofluidic devices in polymers, fluidic transport phenomena in polymeric materials and finally, some compelling applications where polymer-based nanofluidics have been or potentially could be employed. As a final note, there has been a wealth of literature focused on the fabrication and applications of nuclear-tracked polymer-membrane nano-conduits. We have classified these as vertical devices, in which the nanofluidic via is oriented orthogonal to the plane of the substrate. We will not include a description of these devices in this review. However, the reader is referred to several reviews dealing with this type of devices.[4,20,21] Instead, we will focus on horizontal devices, in which the nanofluidic via is oriented parallel to the substrate's surface.

1.1 General properties of polymers

There are two general categories of polymeric materials that have been used in nanofluidic applications: (1) elastomers and (2) thermoplastics. Elastomers are amorphous polymers with a low to moderate number of cross-links between polymer chains. While the low Young's modulus ensures large deformation upon application of an external load, covalent cross-links help elastomers return to their original shape upon release of the load. On the other hand, thermoplastics are usually linear or branched polymers with higher molecular weights and Young's moduli. Polydimethylsiloxane, PDMS, is a good example of an elastomeric material, while examples of thermoplastics are poly(methyl methacrylate), PMMA; polycarbonate, PC; and cyclo-olefin-copolymer, COC. Some of the physiochemical properties of common polymers used for nanofluidics are shown in Table 1. For comparison purposes, we have also included the physiochemical properties of glass (Table 1). As can be seen, polymers have a diverse range of properties that are critical not only in terms of their mechanical properties associated with the ability to fabricate nanostructures (glass transition temperature, T_g; melting temperature, T_m; coefficient of thermal expansion, CTE) using injection molding or hot embossing, but also their operational characteristics in terms of nanofluidics (optical transmissivity and refractive index). The major differences between most polymers and glass is the substantially lower T_g and T_m of polymers, providing the ability to use nanoreplication to directly produce the prerequisite structures and also assemble devices, where the assembly consists of enclosing the fluidic network using for example thermal fusion bonding with a temperature close to the material's T_g.[22,23] Another sharp contrast between polymers and glass is the lower Young's modulus of polymers, which in the case of thermoplastics is about one order of magnitude smaller, but in the case of elastomers this can be as much as 6 orders of magnitude smaller. This value can be critical, because lower Young's moduli can result in nanostructure collapse during thermal/pressure operation of the finished device or during assembly (see Sections 2.2.1, 2.2.6, and 2.3.4).

1.2 Surface modification of polymers

Another interesting property of polymers is their diverse chemistries, which is determined by the monomer units comprising the polymer chains. For example, PMMA possesses functional groups on its backbone consisting of methyl esters while for PC, these functional groups are carbonates. In the case of glass materials, the functional groups are primarily

silanols. As such, a diverse range of surface modification chemistries can be used for polymers to generate functional surfaces appropriate for the intended application,[18,19,24] which can consist of the surface immobilization of biological agents for recognition (nucleic acid probes, antibodies, *etc.*),[25–32] formation of biocompatible surfaces (*i.e.*, surface wettability),[33–37] immobilization of catalytic enzymes for solid-phase bioreactors,[38,39] or solid-phase molecular extractions.[40–42] In addition, simple surface modification protocols can be used to generate functional groups through the use of ultraviolet (UV)-activation,[43–45] plasma oxidation,[46–51] reactive ion beams,[52] microwave-oven generated plasmas,[53] atom-transfer radical polymerizations,[54] and layer-by-layer techniques.[55–58] In the case of glass-based materials, the major surface modification protocol takes advantage of the silanol groups and attaches chemical moieties to this surface through siloxane-based chemistry, which in many cases requires a cross linking agent, such as aminopropyltriethoxy silane (APTES). Unfortunately, this chemistry is susceptible to hydrolytic cleavage at extreme pH values. In contrast, polymer surface chemistries can utilize not only siloxane linkages, but also imine or amide-based linkages as examples.

Common modification protocols employed for polymer surfaces use UV or plasma oxidation of the material, which generates a host of oxygen-containing species, such as alcohols and different carbonyls (aldehydes, ketones and carboxylic acids).[43] In fact, in some cases UV/plasma modification protocols are used to assist in the assembly of the nanofluidic device by lowering the T_g of the exposed material, which permits low-temperature thermal fusion bonding of a cover plate to the substrate minimizing nanostructure deformation.[1,59–61] Unfortunately, some of these modification processes can also alter the surface morphology. For example, Fig. 1 shows tapping mode AFM images of PMMA surfaces treated with either UV radiation or an oxygen plasma.[49,62] In both cases, the root-mean-square (RMS) roughness was found to increase when the material was treated with plasma or UV light. The treated material was found to have an approximately 10 nm increase in its RMS roughness compared to the native material. Therefore, if the substrate containing the nanostructures must be treated with either a plasma or UV light to assist in assembly or to generate surface functional scaffolds for further elaboration, the dose must be carefully controlled to minimize nano-scale roughness increases that can affect the operational characteristics of the nanofluidic device.[62] In the case of glass-like structures, the use of plasmas or UV light is not necessary to generate an activate surface to allow for functionalization and as such, the surface roughness is basically a function of the starting material.

2. Fabrication of nanochannels and nanoslits in polymers

The production of nanoslits and/or nanochannels in polymer materials, whether it be elastomers such as PDMS or the more brittle materials such as thermoplastics, can utilize a variety of fabrication modalities, including those that are typically employed for the fabrication of nanostructures in glass, fused silica, or Si. A summary of the various fabrication techniques that have been used to produce nanostructures in polymers is shown in Table 2. There are several important distinctions that can be noted from this table as opposed to the fabrication of glass, Si or fused silica-based nanofluidic devices: (1) in some cases, one can produce microchannels in the substrate and then apply a stress to the material

to generate the desired nanostructures. (2) Instead of direct writing the nanostructures into a substrate, the demanding steps of nanostructure production using EBL or FIB can be undertaken on a master or stamp, which is then used to produce final parts in the desired polymer; this is basically a nanoreplication or nanomolding process. The primary advantage of the processing strategies depicted in Table 2 is that nanofluidic devices can be produced in a high volume and at low-cost as opposed to direct write fabrication methods typically used for glass-like nanofluidic devices. In this section, we will introduce the concept of nanomolding and then discuss the various techniques used to fabricate nanoslits and/or nanochannels in elastomers, primarily PDMS, and then various thermoplastics.

2.1 Introduction to nanomolding

The deformability of polymers, especially at elevated temperatures, has made these materials to be routinely used for molding of microscale components in industrial production processes for decades.[63] Various molding tools have been developed, which can be used for hot embossing, injection molding, compression molding, thermal forming, casting *etc*. However, only recently has molding demonstrated its capability for producing nano-scale patterns.[64,65] After the pioneering work on nanoimprint lithography (NIL) by Chou *et al.* demonstrating patterns of 25 nm diameter holes in a PMMA film and the subsequent fabrication of metal pillars by metal deposition and lift-off,[64,65] considerable efforts have been devoted to overcome many challenges associated with NIL. Such efforts include understanding fundamentals related to the process, such as polymer flow behavior during molding and stress and deformation of molded polymers during demolding,[66–83] developing optimal materials applicable to the NIL process,[84–95] overcoming the overlay issue,[96–104] fabricating reliable stamps with sub-100 nm features,[105–122] and improving anti-stick coatings.[123–129] NIL has become very successful in patterning structures to sub-10 nm scales,[64,130–132] with the ultimate resolution seemingly determined by the minimum feature size associated with the molding tool.[133] This is the driving force behind the growing efforts of using NIL to produce nanofluidic devices because it can potentially produce multi-scale structures in a relatively high production mode over large areas and do so at low-cost. Readers who are interested in the NIL technology are referred to recent reviews and books.[134–139] Here, we will briefly give some insights of NIL, which are needed in order to apply this technology to the fabrication of nano-based fluidic structures in polymers.

NIL or hot embossing utilizes the rapid change in viscosity (or modulus) of a polymer around its T_g. Fig. 2 shows the typical behavior of the storage modulus *versus* temperature for thermoplastics. The conventional NIL process starts with heating a polymer substrate above its T_g. Then, a hard stamp or molding tool with the desired nanostructures on its surface is pressed into the softened substrate, which forces the resist to flow into the cavities of the stamp structures. After conformal molding, the stamp/substrate assembly is cooled below the substrate's T_g and the stamp is released from the molded substrate. The term “nanoimprint lithography” is considered a special subset of “hot embossing” to indicate the formation of nanostructures. However, for many cases, the two terms are used without distinction.

The flow behavior of a polymer at a molding temperature, usually 50–70 °C higher than its T_g, is determined by the interplay of thermal and mechanical properties of the polymer substrate, wettability of the polymer on the stamp surface and the geometries of the stamp structures. Basically, polymers suitable for NIL are those which allow for sufficient flow for conformal molding at the process temperature and pressure while during demolding, a high modulus is desired to ensure that the deformed polymer patterns sustain detachment of the stamp without damage. Stamp geometry (*i.e.* distribution of stamp cavities and protrusions on a stamp surface) also has a significant role in polymer filling during NIL, and thus should be carefully considered in the design of the stamp and process parameters.[68,71,78–80,137] A general rule on polymer filling is, the shorter the transport distance of the polymer, the faster the filling of stamp cavities under identical imprinting conditions. As an example, large, isolated recessed features surrounded by a large unstructured area requires a long time for complete filling. Also, when patterns with different sizes and densities are present on a single stamp, there is a local variation of stamp sinking velocities resulting in local bending of the stamp during NIL, and thus surface curvature in the imprinted polymer substrate.[137] The polymer or substrate properties can also affect molding fidelity, such as its molecular weight.

While fast molding is important to improve the yield of the process, the process step that determines the success of imprinting high aspect ratio structures is demolding, a process to separate the molding tool from the patterned material. Most structural damage of the imprinted patterns occur at this step. Demolding is a process that involves overcoming all levels of chemical and mechanical interactions between the stamp and the substrate formed by the process history and properties of materials involved. Such interactions include thermal stress generated due to mismatches of thermal expansion in the tool/substrate during the cooling step, adhesion at the tool/substrate interface and friction occurring at sidewalls of the tool/substrate interface during demolding. Demolding failure will occur when stress at the tool/substrate interface becomes larger than the yield strength (σ_Y) of the substrate. Demolding is usually performed at an elevated temperature but still in the glassy state below the T_g of the polymer. Low temperature demolding requires large demolding forces because thermal stress generated during cooling is proportional to ΔT, which is equal to $T - T_g$. On the other hand, at high demolding temperatures, the molded polymer structures are susceptible to deformation during demolding. For PMMA with a $T_g \approx 105$ °C, an optimal demolding temperature has been reported to be around 70 °C, as determined by demolding force measurements and verified by finite element simulations.[140] Efforts to improve demolding processes have been mainly devoted to decreasing the tool/substrate interface energy by: (1) modification of the surface properties for tools by applying an anti-adhesive coating;[86,92,94,124,125] and (2) development of new imprint substrates with anti-adhesive properties.[92,141–143] When the molding tool is made of either silicon or silicon oxide, a coating with fluorinated silane molecules has proven to be an excellent solution to improve the anti-adhesion properties of the tool's surface due to their low surface energy and stability of the bonding. Fluorinated silanes with different carbon chain lengths and silane head groups are readily available. The silane chemistry can be applied to other tool materials, such as nickel, by introducing a very thin intermediate layer (~ 10 nm) of silicon dioxide by sputtering prior to the silane coating.[124] Fluorinated diamond-like carbon (DLC) coatings

have also been employed as a release layer due to its low reactivity to polymer chains.[144–147]

Studies on stress and deformation behavior during demolding provides strategies to improve the demolding process.[140,148–152] For example, high stress concentration usually occurring in the outer most structures indicates that important active structures can be protected during demolding if auxiliary structures are designed and added around the active structures. Also, slightly tapered or rounded stamp structures have been found to significantly help reduce demolding force.

As discussed, the stress generated during molding due to the contact between two dissimilar materials, such as the tool and polymer substrate, inevitably produces undesirable deformation in the molded patterns like warping and a non-uniform residual layer in addition to incomplete filling and ripping of structures. Such deformation in the molded polymer substrate can be tolerated for micro-scale components. However, when nanopatterns are present, particularly when a low number of nanopatterns are surrounded by large micropatterns as is the case for many nanofluidic devices, the deformation is not tolerable, making it difficult to achieve good sealing in the subsequent assembly process. Excessive surface roughness on the stamp surface and inclusion of contamination during the process are also detrimental to nanofluidic structures. For these reasons, most nanofluidic structures fabricated *via* NIL have been formed in a thin layer of thermoplastic polymer spin-coated onto a hard substrate or in an underlying Si or quartz substrate *via* pattern transfer.[153–159]

2.2 Elastomeric materials

Elastomers, although widely used for microchannel fabrication,[47,160] have generally been considered problematic as nanochannels or nanoslits because of their deformability and tendency to collapse. Recently, there have been efforts aimed to overcome or even take advantage of the deformable nature of elastomers to form functional nanochannels and nanoslits. Various categories of nanochannel fabrication have been developed using the elastomer PDMS that we will describe here. We note that there are also a number of nanopores[161] embedded in PDMS structures that have been reported in the literature. In this review, we will not describe such structures.

2.2.1 Collapse of elastomers with low Young's modulus—The multiple orders of magnitude lower Young's modulus compared to glass and Si is a major challenge for construction of nanochannels using elastomers (Table 1). Unwanted elastomer collapse often occurs (Fig. 3) and has traditionally been pointed out as a problem. One of the early studies related to elastomer collapse mechanisms used a PDMS stamp with a Young's modulus of less than 1 MPa.[162] The authors analyzed various types of stamp deformations such as roof collapse, lateral collapse, smooth surface asperities, punch buckling and explained the stability criteria in terms of stamp features and Young's modulus. Here, “punch” refers to the pillars of material between void spaces that function to suspend the stamp structure. Focusing on the adhesion between a PDMS stamp and a substrate, Huang *et al.* and Zhou *et al.* reported the mechanism of “roof collapse” and derived a scaling law to prevent unwanted

roof collapse (Fig. 3a).[163,164] Taking the modulus mismatch between the PDMS stamp and the substrate, the investigators showed that the normalized work of adhesion, $8\alpha\gamma_w/2E'h_p^2$ and geometrical features, *w/a*, were important in determining roof collapse. Here, *E* denotes the Young's modulus of PDMS, $E'=4/3E$ and denotes the plane-strain modulus, γ_W is the work of adhesion between the stamp and the substrate, 2*a* is the punch spacing, h_P is the punch height and 2*w* is the punch width. This analysis results in three regimes of roof collapse: no collapse (weak adhesion), meta-stable collapse, and stable collapse (strong adhesion).

Channel collapse can be useful when controlled. Huh *et al.* analyzed triangular nanoslits and determined the normalized closure distance, c_c/a, (Fig. 3b) as a function of, $E_2h^2/\gamma a$, E_1/E_2, and σ_a/E_2, where E_1 denotes the plane-strain modulus of the oxidized layer, E_2 is Young's modulus of unoxidized PDMS, γ is the surface energy of the nanochannels, c_c is closure distance, σ_a is the remote applied compressive stress, *h* is height, h_f is the thickness of the oxidized layer and 2*a* is the base length of the cross section.[165] These material properties of elastomeric triangular nanoslits allow size-adjustable channel collapse upon application of an external force, however, these inhibit spontaneous channel collapse. This notable characteristic not only applies to crack-induced PDMS nanostructures but can also be generalized to many elastomeric nanoslits and nanochannels. An interesting aspect of triangular nanochannels is that they can partially collapse to different degrees of closure depending on the material property as well as external forces applied. In comparison, roof collapse of rectangular nanochannels is typically an all or nothing phenomenon; either the roof adheres to the bottom of the substrate and collapses or the roof does not adhere to the bottom of the substrate and is suspended.

2.2.2 Tunable PDMS crack-induced nanochannels/nanoslits—One of the early sub-100 nm nanofluidic structures made with PDMS were triangular cross-section nanoslits generated by fracture of surface oxidized PDMS structures (see Fig. 4a).[165] Surface oxidation of PDMS, for example using a plasma etcher, increases the modulus of the surface PDMS layer generating a modulus mismatch between the surface and the bulk polymer. This material property mismatch provides the foundation for crack formation on the PDMS surface. Thus, an array of parallel cracks was created on the plasma-oxidized PDMS layer by an applied uniaxial tensile strain. The pattern of cracks can then be transferred to UV-curable epoxy, which can be used as a master mold. A separate PDMS structure was made from this epoxy mold and sealed with a flat PDMS slab using plasma oxidization. A key requirement for this process was to find mechanical properties of materials that avoided spontaneous nanostructure collapse, but maintained sufficient elasticity to allow for reduction of the nanoslit cross-section upon application of an external force to reversibly convert it into a nanochannel (Fig. 3b and Section 2.2.1). Sealed crack features formed triangular normally-open nanoslits with widths of ~690 nm and heights of ~80 nm. Closure into nanochannels and re-opening back to the larger cross-section nanoslit structures was reversibly controlled by application and removal of pressure on the device. These deformable nanoslit/nanochannel structures have been used for reversible capture of nanoparticles by nanochannel closure induced by application of an external force and subsequent release of the nanoparticles upon removal of the external force.[165,166] The

method has also been demonstrated for nanoscale polymer synthesis, particle sieving and reversible stretching and unstretching of single DNA molecules.[165]

Recently, Mills *et al.* published a variation to this concept of fracture-based nanofabrication by utilizing tunnel cracking rather than surface cracking (see Fig. 4b).[166] This fabrication method is based on crack formation in oxidized PDMS, however, does not require transfer of structures to an intermediate epoxy mold. This is because rather than generating crack features on a surface, then sealing the features against another slab of PDMS to create a closed channel structure, bonding of two PDMS structures is performed first followed by formation of tunneling cracks. In this procedure, a thin flat PDMS membrane and a thicker PDMS slab that contained two microchannel structures were plasma-oxidized and bonded to each other. Subsequently, a uniaxial force was applied to the bonded structure to generate cracks that tunnelled through the brittle layer at the bonding interface. The ordered array of cracks that tunnel through the brittle bonded interface generated size-adjustable diamond-shaped cross-section channels. The cross-sectional dimensions of these conduits could be reversibly adjusted by the amount of external strain applied, where increased stretching leads to larger cross-sectional areas. Optical imaging, electrical resistance measurements and nanoparticle trapping experiments showed that the cross-sectional areas of these channels can be modulated from being completely closed when no strain was applied to having micron-scale cross-sectional dimensions when extensively stretched. Compared to the normally-open triangular nanoslits described previously that required application of external forces to *narrow* them down to nanochannels, these tunneling crack nanochannels have the advantage that they are normally-closed. This feature eliminates unwanted PDMS collapse as well as clogging problems because nanochannels can be *widened* when desired by stretching the device.

2.2.3 Wrinkle-induced nanoslit fabrication—Due to surface stiffness changes and the need to release strain, sinusoidal wrinkle patterns were generated when a sheet of stretched PDMS was exposed to an oxygen plasma[167] or UV/ozone (UVO) and then relaxed.[168] The height and the width of the sinusoidal wrinkle patterns were governed by wave amplitude and wave length. The wave length of the formed structures was dependent on the ratio of elastic moduli of the film and the substrate. Because the thickness of the brittle layer can be regulated by the duration of oxidation treatment, wave length can also be controlled by different plasma/UVO exposure times. The amplitude of the wrinkle structures could be modulated based on the applied strain. This surface buckling phenomena has been used to fabricate nanoslits by Chung *et al.* (see Fig. 4c).[169] PDMS membranes were stretched and exposed to oxygen plasma. Wrinkled PDMS membranes were created when the strain was slowly released. Nanoslit structures referred to by the authors as wrinkle nanochannels (WNC) resulted by bonding the wrinkled PDMS membranes with another oxidized PDMS layer, which contained microfluidic structures. This wrinkle-induced nanoslit fabrication technique has merits of enabling adjustment of the size of the nanoslits formed by controlling the wave length and wave height through fabrication parameters, such as the amount of surface oxidation and the degree of strain. The size of wrinkle-induced nanoslits ranges from tens of nanometres to 2500 nm in width and from tens of nanometres to approximately 500 nm in height.

2.2.4 Sacrificial electrospun nanofibers—Electrospinning produces nanofibers derived from polymer solutions. With an adequate applied electrical field, a droplet of polymer solution at an electrified tip is charged and stretched because of electrostatic repulsion. The droplet generates a “Taylor Cone” from which an electrified liquid jet erupts. The jet dries during flight as it heads towards a grounded substrate resulting in nanofibers. Based on this technique, Bellan *et al.* built sub-micron channels in PDMS using water-dissolvable electrospun nanofibers as sacrificial structures (see Fig. 4d).[170] A PDMS mixture was poured onto a pre-featured silicon substrate with water dissolvable polyethylene oxide (PEO) nanofibers and cured at room temperature overnight. A low curing temperature was used to prevent premature melting of the PEO. After the PDMS structure cured, it was peeled off of the substrate and the PDMS slab soaked in water to dissolve PEO fibers in the PDMS slab. Sub-micron sized channels were left in place of the PEO nanofibers. The channel fabrication was completed by bonding it to a glass substrate using plasma oxidation. Features transferred to the PDMS from the Si substrate served as reservoirs. The measured average diameter of the resulting channels was 455 ± 16 nm and reflected the original structure of the electrospun nanofibers.

2.2.5 PDMS film deformation—Park *et al.* demonstrated a nanochannel fabrication method using deformation of a thin PDMS film (Fig. 4e).[171] Triangular nanochannels were formed between a PDMS film and the sides of a structure fabricated by reactive ion etching (RIE). Specifically, Si structures were prepared using a thin Cr layer pattern followed by RIE with CF_4 gas. Control of the etching time was critical to determine the final height of the structures. After additional steps to make inlet and outlet structures, the fabricated features were sealed to a thin PDMS film by plasma oxidation. Because the thin PDMS film was deformable, the shape of the film conformed to the structure and nano-sized gaps between the structure and the film were generated. In this way, nanochannels were formed without the need of EBL or FIB milling.

2.2.6 “Roof collapse” PDMS nanochannels—In general, nanoslit and nanochannel fabrication with compliant PDMS is challenging because of structural collapse (*e.g.* Fig. 3a). However, Park *et al.* described a nanoslit fabrication technique that actually took advantage of this mechanism (see Fig. 4f).[172] Nanospatial gaps were formed at corners of microfluidic channels through “roof collapse”. The types of submicron channels and slits formed by collapse of microchannels of a given material stiffness were dependent on the geometry of the microchannel. In the work by Park *et al.*, stable high-yield submicron channel and slit formation occurred for a starting microchannel width (a) to height (h) ratio of $a/h^2 \approx 0.2$. For the preparation of the initial microfluidic channel master, precise photolithographic methods were used that incorporated thin photoresist layers or metal deposition. The nanoscale height precision was important because the thickness of the channel master determined the size of the resulting nanoslits and channels. Once a precise master mold was made, PDMS replicas were produced from the master and bonded to a substrate by plasma oxidization. Roof collapse occurred spontaneously to generate nanoslits and channels at the microchannel corners. The advantage of this fabrication method was that nanoslits of arbitrary shapes, not just straight line patterns, could be made. The range of sizes of the nanoslits and submicron channels reported was 60–1000 nm in height.

2.3 Thermoplastic materials

Any nanofabrication technique that has demonstrated the capability for fabricating nanochannel/nanoslit structures in thermoplastics can be used for the fabrication of nanofluidic devices. However, for fluidic applications there are additional constrains in the selection of the appropriate fabrication method. These constraints arise mainly from the requirement of forming enclosed channels and deformability issues associated with thermoplastics. For example, to bond a cover plate made of the same polymer material as that of the substrate, the surface of the substrate involved in the bonding will result in a reduction of nanochannel depth in the enclosed device. Thus, nanochannels with low aspect ratios and rounded cross-sectional profiles may not be suitable for nanofluidic applications. Also, nanochannel/nanoslit-based fluidic devices usually consist of mixed-scale structures containing an array of nanochannels and micro-scale channels as well as large reservoirs serving as the inlets and outlets for reagents. Therefore, the nanofabrication technique should allow for either hierarchical or parallel combinations with various micromachining techniques. In this regard, the overlay accuracy between nanochannels and the microfluidic network must be considered. In this section, we will limit our discussion to those fabrication techniques employed in the fabrication of enclosed nanochannel/nanoslit fluidic devices in thermoplastics.

2.3.1 Beam-based nanolithographic methods—Energetic beam-based nanolithography methods, represented by EBL and FIB milling, are the most common techniques for patterning nano-scale features with arbitrary designs.[173–181] In EBL, patterns are directly defined by scanning focused electron beams onto a thin resist layer, which creates a latent image by chemical development. FIB milling makes use of Ga^+ ions to physically remove materials with a spatial resolution of 20–30 nm. Despite their intensive use in nanoelectronics, these techniques have seldom been used to create nanochannels directly into polymer substrates, which is most likely due to the difficulties associated with the formation of well-defined nanochannel patterns and enclosed fluidic devices following the patterning process. Sub-100 nm patterns formed by EBL usually have low aspect ratios and Gaussian sidewall profiles and this makes the subsequent bonding/assembly process difficult. FIB milling directly into polymers for nanostructure fabrication is still at a very early stage of development due to:[182,183] (1) chemical changes induced in the polymer after direct milling arising from interactions with the impinging high energy ions; (2) charge build-up due to the insulating nature of the polymers; and (3) localized heating due to the low thermal conductivity of the material. Therefore, rather than direct patterning into polymer substrates, EBL and FIB have been used as a means of defining nanostructures in a thin resist layer, which are then transferred to an underlying hard substrate, such as Si or quartz-based nanofluidic chips,[154,184] or for imprint stamps containing nanofluidic structures.[159,185]

As opposed to EBL, proton beam writing can create straight-walled, high aspect ratio nanostructures because a proton is more massive than an electron and, therefore, deviates much less as it penetrates matter.[186,187] Shao *et al.* demonstrated the fabrication of enclosed nanochannels with 200 nm wide and 2 μm deep structures in a thick PMMA resist layer spin-coated onto a Kapton film using proton beam writing coupled with thermal fusion

bonding (see Fig. 5).[188] The use of the flexible Kapton film as a substrate for the nanofluidic chips promoted uniformity of contact pressure over large areas during thermal bonding. Proton beam writing has the potential for rapid and cheap prototyping of 3D micro/nanostructures for research and development purposes and also for the fabrication of high resolution 3D stamps for hot embossing.[106]

Femtosecond laser beams have also been reported in fabricating channels with sub-micrometre cross sections. Yamasaki *et al.* demonstrated the fabrication of sub-micron channels in PMMA films in a single processing step, where a femtosecond pulsed laser beam was scanned in a 3D pattern within a 100 mm thick PMMA film.[189] Both axial lengths of an elliptical cross section close to 200 nm were achieved with a pulse energy of 8 nJ. Channels formed in the PMMA had walls of densified material relocated from the channels' core so that the etch resistance near channel walls was larger than that of the bulk PMMA. Combined with selective etching, this method offered the ability to produce polymer nanotubes. Because enclosed nanochannels were formed in a single processing step, bonding a cover plate was not required, which reduced device assembly steps and minimized nanostructure deformation induced by the bonding process. However, the minimum width in this patterning process was limited to a few hundred nanometres.

2.3.2 Nanoimprint lithography (NIL)/hot embossing—As noted previously, the strong drive of molding technology for producing nanofluidic devices is due to its ability to mass produce parts at low-cost and the diversity of materials that can be chosen as substrates for molding. In this section, we will review some of the work that has been directed toward producing polymer-based nanofluidic devices using NIL as the fabrication protocol.

In work by Abad *et al.*,[153] an array of nanochannels were first produced by nanoimprinting into a thermoplastic polymer resist layer, which were then subsequently transferred to the underlying Si substrate using RIE. Then, the microfluidic structures were added by additional photolithography and RIE steps. Similar approaches have been considered by other groups to produce hierarchical nanofluidic structures.[154,156–158]

Imprinting entire fluidic structures in a single step requires fabrication of imprint stamps with multi-scale structures using various micro- and nanofabrication techniques.[155,159] Thamdrup *et al.* demonstrated the production of a nanochannel chip by means of single step imprinting with a stamp having both nanometre and micrometre protrusions.[159] The protrusions in the stamp were hierarchically fabricated in a SiO_2 layer *via* EBL and photolithographically in a sol–gel resist, which were then transferred to an SU-8 layer *via* imprinting. Then, a simple thermal polymer fusion bonding process was used to seal the imprinted fluidic structures.

Chantiwas *et al.* demonstrated the use of sequential imprinting processes to produce nanoslit-based fluidic devices in different polymer substrates (PMMA, COC, and PC) used for DNA stretching.[59] After formation of the microfluidic vias using hot embossing with a metal molding tool, nanoimprinting followed in order to produce an array of nanoslits in pre-patterned substrates. Critical in this method was preventing the undesired deformation of the pre-patterned microfluidic vias by the second nanoimprinting step. For that, a

significantly lower temperature (110, 130, and 147 °C for PMMA, COC and PC, respectively) was used for the nanoimprinting step compared to that used for hot embossing to prepare the microstructures (160, 175, and 190 °C for PMMA, COC and PC, respectively). The authors also showed production of the entire fluidic devices by single step imprinting using a PDMS stamp. The fabricated nanoslit chips were enclosed with a thin polymer plate bonded to the molded polymer substrate via thermal fusion bonding.

Guo *et al.* have shown that nanoimprinting can be used to enclose nanochannel networks.[190] Their method utilized incomplete filling of molding tools usually occurring when the thickness of a resist layer is much lower than the height of a template. The PMMA nanochannels were made by NIL, in which a Si or glass template was fabricated using NIL structuring of a resist, standard metal deposition, liftoff and dry etching of the substrate to form nanopatterns. They demonstrated that the height of enclosed nanochannels could be controlled by the initial thickness of the PMMA layer and the depth of the nanochannel template.

As noted previously, most nanochannels fabricated with NIL have been formed in a thin resist layer coated on a hard substrate, such as Si or quartz, with the patterns subsequently transferred *via* RIE into a hard substrate; little has been done to form fluidic nanostructures in the bulk polymer directly. Abgrall *et al.* employed hot embossing with two levels of applied force (2 kN and 7 kN) into 1 mm thick PMMA cast sheets with a Si mold fabricated using photolithography and RIE.[191] The chip was then sealed using thermal fusion bonding. They demonstrated an array of enclosed nanoslits with a width of 10 μm and a depth of 80 nm. The critical dimensions (width-to-depth) of nanoslits that could be sustained without collapse were determined by considering the competition between van der Waals forces and the stiffness of the material.[191,192] In the work from Studer *et al.*, nanochannels in polymer substrates were formed by hot embossing of PMMA pellets between a Si mold and a dummy Si wafer followed by thermal fusion bonding with another polymer sheet for enclosing the fluidic network.[193]

Silica nanowires have also been used as templates for the fabrication of isolated nanochannels by placing them between a glass wafer and a PC substrate.[194] The silica nanowires were made by tapering single-mode optical fibers to the desired diameter in an alcohol flame. The wires could be positioned on the glass plate using the probe tip of a scanning tunneling microscope. Following hot embossing, which embedded the wire into the PC, the silica nanowires could be removed from the substrate by etching in hydrofluoric acid. The PC channels were subsequently enclosed using a PDMS cover plate, which also contained microchannels. Channels with widths down to 100 nm could be formed using this technique with lengths up to several millimetres. However, this method could not produce vertical sidewalls and was limited to the formation of simple fluidic architectures (*i.e.*, straight channels).

Direct nanoimprinting into polymer substrates using a Si, quartz, or metal stamp can lead to rather severe, undesired deformation of channels and the entire chip can show warping and/or local substrate bending, making it difficult to generate a tight seal between the fluidic substrate and cover plate.[190,195] The stamp lifetime is also an issue because the expensive

nanostructured molding tool can be damaged due to high stress generated during the imprinting process. In addition, differences in the thermal expansion coefficients between the polymer substrate and the nanoimprinting tool can lead to replication errors.

In an effort to reduce undesired deformation and stress in molded patterns as well as the imprint tool, Wu *et al.* utilized an imprint tool made of a UV curable polymer on a glass substrate to directly nanoimprint structures into a PMMA substrate.[196] The Si master, fabricated by a combination of two sets of photolithography/RIE and FIB milling, consisted of an array of nanochannels, micro-scale channels and reservoirs for inlet and outlet of reagents. The microchannels possessed a depth of 10 mm with a gradient interface as the inlet to the nanochannels where the microchannel depth was reduced to 500 nm. The Si master, with the same polarity as the final fluidic structures, was first replicated into a UV curable polymer coated onto a glass substrate using UV NIL. The pattern in the UV curable polymer layer was then used as a stamp to imprint structures into PMMA substrates. Fig. 6a–c shows SEMs of a Si master, polymer imprinting stamp, and imprinted PMMA using the polymer stamp, which showed good replication fidelity. Also shown in Fig. 6(d) and (e) are nanochannels produced in quartz prepared *via* direct writing into the substrate using a Ga^+ ion beam (FIB milling). From a dimensional perspective, both direct FIB milling and NIL can produce nanochannels with the designed dimensions. In these examples, topographical features on the channel floor could not be interrogated. One subtle issue that can arise using direct FIB milling is ion implantation within the substrate being milled, which would not be present for the polymer channels fabricated *via* NIL even though the Si master was prepared *via* FIB milling. Polymer stamps significantly improved the demolding step during the imprinting process in two ways: (1) thermal stress generated during the cooling step was significantly reduced due to the similar thermal expansion coefficients of the stamp and substrate. (2) Force of adhesion at the stamp/substrate interface, which depends on Young's modulus of the stamp and substrate, was reduced due to a lower Young's modulus of the polymer stamp. The stamp structures were deformed by the application of high pressure during the nanoimprinting process with a polymer stamp of low Young's modulus. Therefore, it was necessary to find an optimal resist composition, which provided both good demolding characteristics and replication fidelity. Additionally, polymer stamps could be repeatedly produced by replication from the original Si master, significantly increasing the lifetime of the expensive Si master patterned *via* EBL, FIB or proton beam writing. Finally, the stamps could be used to produce the desired patterns in a vast array of materials, provided the selected material had a lower T_g than that of the stamp.

Nanotransfer printing,[197,198] a technique of transferring a nanostructured layer from a mold into another substrate by stamping, has been demonstrated as a useful process to fabricate enclosed nano-scale polymer channels. In the process developed by Dumond *et al.*,[195] a thin PMMA film cast on a Si grating mold was subsequently embossed with a second grating mold. The PMMA film with patterns on both sides was then stamped into a Si or indium substrate, which transferred the structured film from the second grating mold into the substrate due to surface energy contrast at the two interfaces. The substrate used for the stamp acted as a cover plate for enclosing the nanochannels, and thus no additional bonding

process was required. The use of a substrate of the same polymer material as the transferred film in order to produce all polymer-based nanofluidic chips would potentially be feasible.

2.3.3 Miscellaneous methods—Several groups have reported the creation of nanoscale depressions in a thin film of thermoplastic using atomic force microscopy (AFM) nanolithography.[199–202] As an example, Tsai *et al.* employed AFM nanolithography with high aspect ratio Si tips to fabricate nanochannels in PMMA with a width of 80 nm and a depth of 30 nm for the fabrication of glucose biosensors.[201] However, the serial process with small scan velocities of 1–10 μm s^{-1} limits the throughput of this process to generate nanostructures over large areas. The maximum channel length that could be produced without break or stitching was also limited by the range of the AFM scanner motion, which was 10–100 μm. Moreover, the nanochannels produced by AFM nanolithography usually possess low aspect ratios and have V-shapes, conforming to the shape of the AFM tips. Also, the material removed by the AFM tip piles up surrounding the indentation, which makes it difficult to form enclosed nanochannels in the subsequent bonding process.

A number of methods, which do not require the use of nano-scale writing tools or a stamp (or mold) with nano-scale patterns have also been developed. Eijkel *et al.* developed a simple method using spin-coating and sacrificial layer etching to fabricate all-polyimide nanoslits.[203] After patterning an aluminium sacrificial layer with micropatterns on the first polyimide film using photolithography and an aluminium etchant, the authors spin-coated a second layer of polyimide on top of the aluminium and first polyimide layer. The thickness of the sputtered aluminium sacrificial layer determined the height of the final nanoslits. The formation of enclosed nanoslits was achieved by etching the sacrificial aluminium layer. The sacrificial layer etching process took about 20 h and was limited by diffusion of both the Al etchant and removed Al in the enclosed nanoslits. This limitation in the sacrificial layer etching process made it difficult to use this method for the fabrication of nanochannels.

Sivanesan *et al.* demonstrated a simple method for fabricating nano-scale channels based on thermomechanical deformation of rigid polymer substrates, mimicking the draw process in the fabrication of silica capillaries.[204] In their work, PC preforms containing microchannels with cross-sectional dimensions on the order of tens of micrometres were controllably deformed by applying a uniaxial tensile force at the T_g of PC (~ 150 °C). This reduced the channel cross section through the Poisson effect. Arrays of parallel nanochannels with critical dimensions down to 400 nm were demonstrated. Fig. 7 shows a fabricated nanofluidic chip made by the mechanical deformation of thermoplastic polymers and electron micrographs showing a single nanochannel. Factors determining the size and shape of the final nanochannels included the pull distance, temperature distribution and location of the original microchannel within the preform. Also, the maximum reduction in channel width and height was found near the edge and center of the preform, respectively. Despite its simplicity and reproducibility, the thermomechanical process is limited to applications where straight channels or an array of nanochannels with equal lengths are required.

The ability to make Si nanoimprinting stamps with high aspect ratios without requiring EBL or FIB was recently demonstrated.[205] In this process strategy, Si ⟨100⟩ stamps were fabricated using KOH anisotropic etching of Si and the local oxidation of Si. The Si

nanoimprinting stamps were coated with 1H, 1H, 2H, 2H-perfluorodecyltrichlorosilane and the imprinting was performed using PMMA substrates. Channels with depths of 1.1 μm and widths of 200 nm were formed (aspect ratio = 1 : 5.5) with the minimum width reported to be 100 nm. The fluidic channels were enclosed using a solvent-assisted method; the substrate was exposed to methanol or toluene vapor, which caused melting of only the top portion of the high aspect ratio structures basically sealing the nanochannel.

Self-organization of materials is a powerful tool to produce nanoscale structures in a cost effective manner, requiring no nanolithographic tools. Faruqui and Sharma demonstrated a simple nanofabrication technique to obtain an array of nanochannels based on stress-induced cracking of thin film microstructures at sharp edges.[206] PMMA micro-scale stripes of triangular cross-section were first produced using incomplete filling and extended annealing. When the triangular gratings were further annealed, cleavage was observed starting on the pointed tips of the triangular stripes in order to relieve the stresses locally built up at the tips. Fabrication of 100 nm wide and 120 nm deep fine nanochannels has been demonstrated with this method. Fabrication routes based on dewetting of polymer films on nonwetting substrates[207] and di-block copolymers in combination with external fields and chemical steps[208–211] have also been developed to produce highly aligned polymer nanochannels. However, these routes are still premature to be used for the fabrication of enclosed nanochannel-based fluidic chips due to difficulties in integrating hierarchical multi-scale structures.

Xu *et al.* developed a lithography-free nanochannel fabrication technique where cracks are induced by swelling a polymer layer on the surface of polystyrene (PS) petri-dish lids (see Fig. 4g).[212] In this procedure, PS petri-dishes filled with an ethanol solution were heated. The heated ethanol stream absorbs on the inner surface of the petri-dish lid, swelling thin layers of the inner PS petri-dish surface. Simultaneously, the process generates a temperature gradient (80 °C to 25 °C) between the inner and the outer surface of the PS petri-dish lid. Upon cooling, the released ethanol from the inner petri-dish lid surface resulted in shrinking of the surface thin film. Due to the anisotropy of PS chains within the petri-dishes, release of stress was biased in terms of direction and induces parallel cracks that were evenly spaced on the surface. The crack array features on the PS petri-dish could be replicated into a polymer mold and further transferred into PDMS. Nanochannel dimensions could be adjusted by choice of temperature, solvent type, solvent volume, heating duration of the original PS cracking step and was affected by the degree of swelling and temperature gradients. Use of ethanol and 80 °C heating were ideal conditions for mild PS swelling and regular crack pattern formation. This fabrication method was related to the cracking fabrication by PDMS stretching except that the surface thin film was strained without direct application of external mechanical forces.

2.3.4 Thermoplastic nanofluidic device assembly—Thermal fusion bonding is a common technique used to enclose polymer-based fluidic devices and is accomplished by carefully controlling the time, temperature and pressure used for bonding a patterned polymer substrate to its cover plate. For microfluidic channels, direct thermal fusion bonding is carried out by heating both the substrate and cover plate to a temperature near or above the T_g of the specific material while applying a pressure to increase fusion contact

force.[61] However, this process can be challenging for enclosing fluidic devices containing nanostructures due to slight bulk polymer flow, which can cause significant nanostructure deformation. Abgrall *et al.* and Chantiwas *et al.* achieved assembly of thermoplastic nanoslits (80 nm and 100 nm deep nanoslits, respectively) by utilizing a protocol employing thermal fusion bonding at a temperature lower than the T_g of the material by using oxygen plasma treatment of both the cover plate and substrate prior to chip assembly.[59,191] Fig. 8 shows the metrology of (a) PMMA and (b) COC nanoslits (see Fig. 8 for chip assembly conditions) assembled at different temperatures. Reduction in the depth of the nanoslits (red traces) when plasma oxidized and fusion bonded at a temperature below the bulk T_g of the material compared to the slits without chip assembly (black traces), which were found to be 6% for PMMA and 9% for COC, respectively. However, thermal fusion bonding close to the bulk T_g of the material (107 °C for PMMA and 130 °C for COC) collapsed the nanoslits by 40% and 60% for PMMA and COC, respectively.

However, thermoplastic structure deformation *via* thermal fusion bonding can be used for tailoring the geometrical properties of polymer structures. Wang *et al.* presented an approach coined ‘pressed self-perfection by liquefaction (SPEL)’ to control trench, line and hole dimensions.[213] By pressing a guiding plate with a smooth surface on top of patterned structures on a substrate, the structure spacing and hole diameter decreased using SPEL. By applying a temperature of 65 °C for 20 min, the grating spacing was reduced from 120 nm to 12 nm using an applied temperature of 100 °C for 0.5 min. The T_g of the material used for these nanostructures was 55 °C.

3. Transport phenomena in polymer nanochannels and nanoslits

There have been several comprehensive reviews on nanofluidic transport phenomena.[1,2,209,210] The major differences that exist between microfluidics and nanofluidics result from electro-kinetic transport mechanisms. The electrical double layer can occupy a large amount of the cross-sectional area of the fluidic via or in some cases, even overlap if the channel dimensions are comparable to the double layer thickness. Therefore, the electrical double layer is critical in determining the characteristics of nanofluidics compared to microfluidics and this is where polymer nanofluidics can be uniquely distinguished from glass or fused silica nanofluidics due to differences in the zeta potential between glass and many polymers. In this section, we summarize nanofluidic principles based on electro-kinetic and hydrodynamic transport phenomena and compare and contrast polymer and glass-based nanofluidics with respect to these transport phenomena. For a more extensive review of transport phenomena in nano-confined environments, the reader can refer to the references listed above.

3.1 The electrical double layer and electrokinetic transport in nano-confined environments

Electrokinetics is a commonly used transport mechanism in nanofluidics due to the fact that significantly smaller pressure drops occur compared to hydrodynamic driven transport and the ability to directionally drive the flow without the need for valves. Electrokinetic transport is typically produced from both the electrophoretic mobility of the molecule being driven through the nanochannel or nanoslit and the bulk electroosmotic flow. Electroosmotic flows (EOF) are highly dependent on the surface charge of the material and this is where

polymers distinguish themselves from glass or fused silica-based substrates; the surface charge for polymers can be highly variable and depends on the substrate material as well as the nature in which it was treated. In most cases, the EOF in polymer-based devices is smaller compared to glass.[19,214]

The surface charge density (σ_s) is described by $\sigma_s = \Sigma_i q_i/A$ where q_i is the net charge of the ion and is given by $q_i = z_i e$, where z_i is the valency of the ion, e is the electron charge, and A is the surface area. Surface charges also result in an electrostatic force, which can play a significant role in the interactions between the transported molecules and surfaces, especially in the case of nanofluidics.

Here we describe the formation of the electrical double layer (EDL) and how it relates to the surface charge density when different materials are used. The EDL is composed of the Stern layer and the diffuse layer and occurs at the solid–liquid interface. The potential distribution of the charged interface in the EDL (ψ) is expressed by the Poisson–Boltzmann equation, $\nabla^2\psi = \frac{d^2\psi}{dz^2} = \kappa^2\psi(z)$, where κ is the Debye–Hückel parameter and z is the surface normal direction. The Debye length, $\lambda_D = \kappa^{-1}$, describes the length where the potential has dropped to e^{-1} of the original potential. By assuming a symmetrical $z_i : z_i$ electrolyte with concentration C_i at 25 °C, the Debye length (m) can be given as $\lambda_D = \frac{3.04\times10^{-10}}{\sqrt{I_s}}$, where the ionic strength is $I_s = \frac{1}{2}\Sigma c_i z_i^2$. For $I_s = 10^{-2}$ M, $\lambda_D = 3.04$ nm, while for $I_s = 10^{-4}$ M, $\lambda_D =$ 30.4nm.

For nanochannels as opposed to microchannels, λ_D/h (h is the width and/or height of the nanochannel or nanoslit) is close to unity (dashed line, Fig. 9), which can have a pronounced effect on the EOF and follows the electric potential $\psi(z)$ profile and will not produce the common plug flow profile associated with electrokinetics in microchannels. At low ionic strength, the electroosmotic velocity (v_{eo}) is dependent on the electric potential distribution $\psi(z)$ as expressed in the equation $v_{eo} = \frac{E_V \varepsilon \varepsilon_0 \zeta}{\eta}\left(1 - \frac{\psi(z)}{\zeta}\right)$, where E_V is the applied electric field, ε is the relative dielectric permittivity, ε_0 is the vacuum permittivity, η is the dynamic viscosity of the electrolyte and ζ is zeta potential, which is the electric potential at the interface of the Stern and diffuse layers. Based on this equation, if one compares v_{eo} at a certain z-position between polymers and glass nanochannels, it can be assumed that v_{eo} will be lower in polymers because ζ of polymers is typically lower than glass.[215,216]

The zeta potential is related to the diffuse layer charge density and can be determined through the electroosmotic mobility,[209,212] and can be changed either using different materials, such as glass or polymers, or by surface treatment of the material, for example through chemical reactions or photochemically-induced surface reactions.[215,217] Kirby and Hasselbrink recently reviewed zeta potentials for different materials, such as Si, glass and fused silica and included information on a variety of polymers, for example PDMS, PC, PMMA, polyethylene terephthalate, polyethylene, polystyrene and polyvinyl chloride.[216] Chai *et al.* reported on zeta potentials of PMMA modified using an oxygen plasma.[218] Oxygen plasma modification is often used for polymer microfluidics and recently, nanofluidics. For example, Abgrall *et al.* reported the use of oxygen plasma treatment for nanoslit preparation in PMMA[191] and Chantiwas *et al.* utilized oxygen plasma treatment for

different thermoplastic nanoslits (PMMA, PC and COC) for chip assembly.[59] Chai *et al.* found that ζ depends on the surface charge density and double layer thickness of different electrolyte solutions.[218]

Table 3 presents ζ and the corresponding interfacial charge density of untreated and 50 s plasma-treated PMMA in different solutions. Plasma-treated PMMA has higher values of ζ and the corresponding interfacial charge density (σ) for all solutions. Increases in ζ of modified PMMA surfaces in water could be due to the generation of charge states arising from plasma treatment or the ionization or dissociation of new functional groups (*e.g.* the dissociation of surface carboxylic acid groups).[218] Effects of oxygen plasma treatment on the EDL and ζ is a complicated process, however, oxygen plasma treatment does lead to a more negatively charged surface. The authors also reported that the EDL contribution to the solid–liquid interfacial tension was negligible.[218] Measurement of ζ for COC compared to glass substrates was reported.[219] By considering hydrophilic/hydrophobic differences between COC and glass substrates and using time-resolved electro-kinetic measurements, ζ of silica was −25.7 mV with a value of −14.1 mV for COC using a 10 mM phosphate buffer (pH 7).

The EDL overlap can also induce concentration polarization effects near the end of a nanochannel. Concentration polarization involves two basic phenomena—ionic depletion and ionic enrichment. Application of an applied voltage, in which the EDLs overlap, results in the selective passage of counter-ions through nanochannels with the migration of co-ions toward the anode. As a result, the concentration of counter-ions decreases near the anodic side of the nanochannel to maintain electroneutrality generating an ion depletion region. The electrical conductivity in the ion depletion region becomes very low; thus, a high electric field is formed near the anodic side of a nanochannel. This electric field induces an excess flux of counter-ions through the nanochannels forming an enrichment effect on the cathodic side. Finally, ionic depletion and enrichment regions are formed at both ends of the nanochannel when a voltage is applied across the channel.

3.2 Hydrodynamic flow in polymer nanochannels

There are basically two different modalities to induce flow in nanochannels hydrodynamically: (1) the use of capillary pressure, which is based on the surface tension forces between the liquid and the surface; and (2) hydrostatic pressure, which requires the use of an external source to force the fluid through the nanochannel or nanoslit. The capillary or Laplace pressure (ΔP_L) can be calculated using the equation, $\Delta P_L = 2\gamma(\cos \theta_C)/r$, where r is the capillary radius, θ_C is the water contact angle and γ is the surface tension of the liquid in air (for water, $\gamma = 0{:}0073 N/m$). As can be seen from this equation, the capillary pressure is dependent on the water contact angle of the substrate material comprising the nanochannel. For example, the water contact angle of glass, PMMA, PC, COC and PDMS are 36°, 67°, 82°, 92°, and 110°, respectively. For a 50 nm channel (aspect ratio ~1) and water filling this channel, the capillary pressure would be approximately 23.4 atm, 11.3 atm, 4.0 atm, −1.2 atm, and −9.8 atm for glass, PMMA, PC, COC and PDMS, respectively. As can be seen, the capillary pressure actually drives the fluid from the channel and towards the inlet for PDMS and COC substrates due to their hydrophobic nature (*i.e.*,

water contact angle >90°) as opposed to glass, which draws the fluid into the channel strongly. However, oxygen plasma treatment can introduce many different oxygen-containing moieties onto the polymer substrate material, and thus lower its water contact angle. For example, COC treated with an oxygen-plasma will produce a surface with a water contact angle of ~23°, which will reverse the direction of the capillary pressure and draw water into the channel.

The liquid position in the channels was modeled using $L=\sqrt{2\Delta PC_{\mathrm{g}}t/\eta}=\sqrt{R\gamma\left(cos\,\theta_{\mathrm{C}}\right)t/2\eta}$, where L is the liquid front position, C_{g} is the shape factor of the channel/slit, η is the solution viscosity, t is time, and R is the hydraulic radius, which is equal to the ratio of the cross-sectional area to the wetted perimeter. Recently, capillary flow in poly(ethylene glycol), PEG, and PDMS nanoslits has been measured. Average flow velocities for 3 mm long rectangle channels were reported as 1.5×10^5, 1.2×10^4, and 6.0×10^2 μm s^{-1} for PEG channels corresponding to hydraulic radii (R) of 34.92, 1.71 and 0.19 μm, respectively. The water flow velocity was measured in PEG nanoslits with dimensions of 4×0.2 μm^2, 4×3 μm^2 and 145×46 μm^2 (width × height) corresponding to R values of 0.19, 1.71 and 34.92 μm, respectively. In the case of PDMS nanoslits, water did not enter the nanoslit with dimensions of 4×0.2 μm^2 (R = 0.19 μm) due to a high flow resistance because of the large water contact angle of PDMS and partial collapse of the nanoslit arising from the low Young's modulus of PDMS. In Fig. 10 is shown a plot of L *versus* $t^{1/2}$ values, which followed that predicted by the equation for Poiseuille flow.[220]

For hydrostatic pressure driven flow, an external source is used to actively pump the fluid through the nanochannel with the flow rate determined by the equation $Q=\frac{-kA}{\eta}\left(\frac{\Delta P_{\mathrm{E}}}{l}\right)$, where k is the permeability, ΔP_{E} is the pressure drop along the nanochannel, of which the length and the cross-sectional area are l and A, respectively. There are two challenges with driving fluids hydrodynamically through nanochannels or nanoslits, the high pressure drop that is associated with the small cross sections of these conduits and also, the capillary back pressure that can be generated for channels with contact angles >90°.

For hydrostatic pressure driven flow, an external source is used to actively pump the fluid through the nanochannel with the transport velocity determined by the magnitude of the external driving pressure and the cross-sectional area of the nanofluidic channel. There are two challenges with driving fluids hydrodynamically through nanochannels or nanoslits, the high pressure drop that is associated with the small cross sections of these conduits and also, the capillary back pressure that can be generated for channels with contact angles >90°. Polymer-based nanofluidic devices are typically limited in terms of their operating pressures due to the poor tensile strengths associated with the cover plate bonded to its substrate.[59] In addition, their low Young's modulus compared to glass-based substrates can give rise to nanochannel deformation when operated with large head pressures, especially when using elastomeric materials such as PDMS.

4. Applications

4.1 DNA stretching/linearization

One application area for nanochannels and nanoslits is DNA stretching/linearization. Analysis of DNA linearization can provide insights into physical properties of DNA, which is interesting for basic polymer physics as well as understanding regulation of gene expression. Linearization of the randomly coiled DNA structure in micro-scale environments is also useful for mapping locations of certain sequences within a strand of DNA as well as for the “direct reading” approaches for DNA sequencing. Examples of the types of analysis that involve DNA linearization include molecular combing,[221] DNA direct linear analysis (DLA),[222] optical mapping,[223] and nano-confinement.[224] DLA and optical mapping both utilize shear stretching of molecules in small channels for the linearization. Molecular combing performs shear stretching of DNA without the use of channels but by using a moving air–liquid meniscus. Shear stretching has the advantage that submicron or micron-scale channels or even no channel setups can be used to obtain a relatively large degree of DNA linearization. The drawback is that the extent of linearization can be variable and as soon as the shear is removed, the DNA molecule will recoil. In DLA, linearized DNAs are imaged while they are being shear stretched as they move through nanochannels. This allows the sequential imaging of multiple single molecules of DNA through a channel. Optical mapping utilizes hydrodynamic forces created within channels to stretch DNA, but then immobilizes the resulting linearized DNA onto a silanized cover slip. Subsequent digestion of these surface immobilized DNAs using restriction enzymes results in an array of DNA fragments that remain attached to the surface. Fluorescent staining results in an optically visible restriction map, where contiguous strands of DNA appear as continuous lines and restriction sites appear as dark gaps that interrupt such lines. Optical mapping is useful because it provides “fingerprints” or “bar codes” unique to the sequences present in the original DNA strands.

In contrast to DLA and optical mapping, which relies on shear stretching, nano-confinement stably maintains DNA in its linearized state even under static conditions. DNA linearization using polymer nanochannels has been demonstrated by Mannion *et al.*, who used PMMA micro- and nanochannels fabricated by EBL.[225] They loaded T4 phage DNA and studied DNA stretching, relaxation, and recoiling in the polymer channels. Li *et al.* fabricated 100 nm nanochannels using a sacrificial polymer poly(butylnorbornene), and showed electrically driven DNA translocation through these channels.[226] Guo *et al.* used PMMA nanochannels made by NIL for DNA linearization. The authors used these devices to demonstrate that the extent of T5 DNA stretching (contour length = 35 μm) was inversely proportional to the size of the nanochannels.[190]

Chantiwas *et al.* recently presented nano-replication of thermoplastic nanoslits using a simple molding tool, which consisted of an optical mask with the Cr layer thickness defining the nanoslit depth.[59] λ-DNA translocation through PMMA and COC nanoslits was reported. Both materials demonstrated voltage-dependent mobilities with higher electric field strengths showing reduced mobilities due to dielectrophoretic trapping, a consequence of the relatively high roughness of the material following imprinting. The extension factors for λ-

DNA in this work were found to be 0.46 for PMMA and 0.53 for COC nanoslits. The degree of extension was suggested to depend on surface energies; oxygen plasma treated COC surfaces have a lower water contact angle (23 ± 2°) compared to PMMA (57 ± 2°) and thus, different surface energies. Therefore, the physical dimensions of the nano-confined environment may not be the only factor influencing extension, but the material properties of the nano-environment as well.

Huh *et al.* described the dynamic modulation of a reversible-controlled nanochannel whereby application of an external pressure causes channel closure, inducing λ-DNA linearization. Fig. 11 illustrates λ-DNA stretched to a length of ~6 μm (30% of its contour length) when initially introduced into PDMS nanoslits (~690 × 80 nm^2) and then linearized to ~14 μm (70% of its contour length) when an external pressure was applied to the device.[165] The ability to dynamically modulate the degree of DNA linearization through modulation of the cross-sectional area of nano-conduits is a unique capability of elastomeric devices.

Thamdrup *et al.*[159] and Park *et al.*[117] approached the relation between the degree of DNA streching and the dimension of polymer nanochannels quantitively using de Gennes's[227] and Odijk's[228] polymer models. These basic polymer theories describe and predict confinement and conformation of DNA in limited spaces, which are smaller than the radius of gyration of the DNA molecule. In the de Gennes's regime, DNA is considered as a series of locally coiled and noninteracting blobs when the average diameter of the space, such as a nanochannel, is larger than the persistence length of the DNA. Odijk's regime, by contrast, models DNA extension in spaces smaller than the persistence length of DNA. In PMMA nanochannels having a width and height of 250 nm, T4 phage DNA was stretched to 20% of its countour length (see Fig. 12).[159] This value corresponded to the estimated value predicted by de Gennes' model. Park *et al.* generated 500 and 100 nm deep nanochannels based on PDMS deformation and stretched λ-DNA in these PDMS nanochannels.[117] They showed that DNA linearization followed de Gennes's model in the 500 nm channels but followed Odijk's model in the 100 nm nanochannels. In a related study by Jo *et al.*, λ-DNA and T4 phage DNA molecules were loaded electrokinetically into a PDMS nanoslit device.[16] They showed that for a given dimension nanoslit, the degree of DNA elongation was inversely dependent on ionic strength.

As can be seen from these examples, the challenge for the use of nanoslits and nanochannels for DNA and chromatin stretching is that a high degree of linearization requires very small channels (<50 nm) but, as the channels become smaller, it becomes more difficult to introduce the biomolecules into the devices. Size-adjustable nanochannels are advantageous because they provide wide channels for easy sample loading as well as narrow channels for extensive DNA linearization. The use of elastomers allows for such modulation, while materials like glass or fused silica do not. In addition, because the degree of linearization is related to the size of the nanochannel, channels with dimensions significantly below the persistence length of the DNA biopolymer do not need to be directly fabricated using EBL or FIB milling. The tailoring of the nanochannel dimensions can be affected by applying a stress to an elastomeric material, which is a reversible process. In the case of non-

elastomeric polymer material, generating channels with dimensions below the persistence length of the DNA can be achieved using self-perfection by liquefaction processes.[213]

4.2 Molecular preconcentration

Sample preconcentration is often required for the analysis of trace constituents in relatively large volumes of samples. Several preconcentration methodologies including field amplified sample stacking,[229,230] isoelectric focusing,[231] electric field gradient focusing,[232] temperature gradient focusing,[233] isotachophoresis,[234] and electrokinetic trapping[235] have been utilized for preconcentration of target molecules using capillaries or microfluidic devices.

Nanochannels and nanoslits have also been utilized for the preconcentration of biomolecules using physical phenomena unique to nanochannels. Most nanofluidic preconcentrations have been performed on the basis of electrokinetic trapping based on the concentration polarization effect as shown in Fig. 13a, because the mechanism can be used for various molecules and buffer systems.[236] Recently, polymeric devices have been applied for the electrokinetic preconcentration of molecules. Kim *et al.* utilized a nanochannel created between a PDMS microchannel and a glass substrate for the electro-kinetic preconcentration of albumin proteins.[237] Lee *et al.* demonstrated the same phenomenon using a nanogap formed by electrical breakdown of thin PDMS walls.[238] They could obtain a 10^4-fold preconcentration of β-phycoerythrin within 1 h. Ion-selective nanoporous materials, such as Nafion polymers integrated into a microfluidic device by microcontact printing[236] or capillary-force-induced self-filling,[239] have also been used as a nanofluidic ion filter for the preconcentration of biomolecules using the ion depletion phenomenon.

Molecular preconcentration using polymeric nanoslits has also been demonstrated. Chung *et al.* utilized nanoslits fabricated by wrinkles in PDMS for concentrating β-phycoerythrin as shown in Fig. 13b.[169] They could preconcentrate the molecules $>10^2$ fold within 10 min. They also investigated the effects of nanoslit dimensions on the efficiency of the preconcentration using a simple prototyping protocol of nanoslits based on wrinkle formation of a PDMS substrate.

Nanochannel preconcentration systems have also been utilized for improving the sensitivity of enzyme activity assays. Lee *et al.* preconcentrated target cellular kinases, such as MK2 and PKA, from HepG2 cell lysates and fluorogenic substrates using electrokinetic trapping.[240] The sensitivity and the velocity of the reaction was enhanced 65-fold and increased 25-fold, respectively. Enhancement of detection sensitivity and dynamic range of a microfluidic immunoassay has also been demonstrated using a nanofluidic preconcentration device. Cheow *et al.* developed a PDMS microfluidic device into which a nanoporous membrane was integrated to increase the sensitivity of a standard enzyme-linked immunosorbent assay for the detection of prostate specific antigen and CA19-9 in serum.[241] They could successfully preconcentrate product molecules using electrokinetic molecular accumulation and obtained ~100-fold enhanced detection sensitivity.

4.3 Molecular separations

The surface-to-volume ratio is large in nanochannels resulting in surface-charge governed transport that offers unique opportunities for charge-based molecular separations. Due to the lithographic processes used to produce the fluidic vias and the small size of the separation platform, a single wafer can accommodate a large number of separation devices appropriate for applications requiring high throughput processing. As the volume required for loading is very small, especially for nano-scale separations, these separations could be utilized for the interrogation of mass-limited samples, for example the analysis of single cells, fine needle aspirates and embryonic organisms. Separations in nanochannels using Si or glass-based materials have been evaluated extensively. Unfortunately, no work has appeared to this point highlighting the use of polymer nanochannel separations. Therefore, we will briefly present work using nanochannels for molecular separations with glass substrates and discuss opportunities polymer substrates may offer. In nanochannels made from Si or glass materials, the electric field associated with the EDL produces transverse ion distributions that depend on species charge.[242] Thus, flow along the channels yields charge-dependent mean axial speeds enabling separation by charge. These charge-based nanochannel separation strategies may be classified into two general categories; (1) nanochannel electrophoresis; and (2) nanochannel chromatography.

4.3.1 Nanochannel capillary electrophoresis—Theories and experimental studies for electrokinetic separations in nanochannels have appeared in recent reviews.[243,244] Electrophoretic motion of molecules and ions in nanochannels requires different perspectives for analyzing the phenomena compared to electrophoresis based on microchannels or capillaries. In nanochannels, effects of the EDL become more significant due to λ_D, which is either overlapped or occupies a significant cross-section of the channel. The EDL induces non-uniform electric fields in the vertical direction to the wall as well, resulting in ionic concentration gradients due to the equilibrium between electromigration and diffusion of ions. This transverse concentration gradient in nanochannels depends on the valence number of ions, the Debye length, surface charge density, and temperature.[242,245]

Channel dimensions also affect molecular motion under an electric field in a nanochannel. In shallow and wide channels, Taylor dispersion of neutral analytes across the channel width is not negligible compared to that across the channel depth due to longer time scales for their diffusion.[246] This effect is also applicable to nanochannels, which are typically fabricated with high aspect ratios. In the case of charged molecules in nanochannels, the equilibrium of their electromigration and diffusion also affect their dispersion because molecular diffusion can be constrained by the non-uniform electric field in the EDL.

Interactions between molecules and channel walls also become dominant at such small scales. Electrostatic interactions of charged molecules with charged walls can affect the separation. The adsorption and desorption of molecules can also influence their transport.[243] For example, Garcia *et al.* observed the separation of rhodamine B (neutral) and Alexa 488 (valence = −2) in channels where the dimension varied from 35 to 200 nm.[247] Here, electrostatic repulsion of Alexa 488 from the negatively-charged walls and the adsorption of neutral rhodamine B to the walls contributed to the separation. The adsorption of molecules

onto channel walls may allow chromatographic separations in nanochannels, which will be discussed in the next section.

In the case of macromolecules, the polarization and steric interactions with channel walls may occur due to strong transverse electric fields and nanometre-scale channel dimensions, which can be on the order of the molecule.[243] The polarization may affect steric interactions of molecules and their transport in the nanochannels. These steric effects may also influence the adsorption/desorption of molecules resulting in the change of molecular motions under the electric field in a nanochannel.

So what are the potentials of doing electrophoretic separations in polymer-based nanochannels? The most obvious difference is that for polymers, their hydrophobic character is different from that of glass-based materials. Therefore, wall-interactions, especially for nanochannels where the surface-to-volume ratio is extremely high, can be more prevalent for molecules that are themselves fairly hydrophobic. In addition, polymers typically show EOFs that are smaller than glass-based devices most likely due to the lower surface charge density of the polymeric material. For example, PMMA and PC have EOFs that are approximately 2×10^{-4} cm^2 V^{-1} s^{-1},[214] whereas the EOF for glass is approximately 4.9×10^{-4} cm^2 V^{-1} s^{-1}. The smaller EOF in many polymers compared to glass would affect the axial migration rate of material through the nanochannel compared to glass-based devices. In addition, the lower surface charge density on polymers would also minimize artifacts due to ion exclusion caused by concentration polarization. Polymer surfaces can be readily modified using either plasmas or UV light and this can have an impact on the surface charge density of the material, which can affect its EOF and/or solute/wall interactions.

4.3.2 Nanochannel chromatography—Nanochannel chromatography or nanochromatography is a new technique where separation of molecules is achieved in nanochannels without the use of a packed column. Packing small diameter columns with silica particles, which has been done in conventional micro-scale separations, is a difficult task. This limitation can be circumvented by reducing the channel size to sub-micron length scales, because the reduced diffusional distance allows the use of open channels for the chromatographic separation without sacrificing chromatographic efficiency. Also, as the hydraulic diameter of the nanochannel is on the order of the EDL thickness, solutes can be separated based on charge.[248]

Kitamori *et al.* introduced a novel technique coined femto liquid chromatography (fLC) for the separation of negatively charged solutes, such as fluorescein (−2 charge) and sulforhodamine B (−1 charge) in a nanochannel using pressure-driven flow.[249] These solutes were separated only in fLC within 30 s and the elution time of fluorescein, which has a higher negative charge, was shorter than that of sulforhodamine B. Here the thickness of the EDL in the nanochannel significantly affected the velocity of the solute. The authors demonstrated that the velocity difference of solutes depended on various factors with the maximum occurring when the ratio of the channel size to λ_D was ~4. If the ratio is too large (large channel size and small λ_D) or too small (small channel size and large λ_D), the charged solutes spread throughout the channel or localize to the channel center due to electrostatic forces resulting in no difference in their velocities.

Polymer nanochannels will offer a unique venue for performing fLC due to the fact that the substrate material can potentially serve as the stationary phase without the need for appending different monolayer assemblies to the support as required for glass to affect the separation. This is a consequence of the diverse surface chemistries associated with different polymeric materials and also, the simple modifications that can be imposed on them using plasmas or UV light.

4.4 Solid-phase reactors

Solid-phase bioreactors consist of two different types; (1) selection of targets from a mixed population, using as an example affinity selection; or (2) enzymatic reactors in which catalytic enzymes convert substrates into products. In either case, the selection element or enzyme are either covalently or noncovalently attached to a solid-support and the targets or substrates are solution-borne and can be driven through the reactor bed either hydrodynamically or electrokinetically. There are several advantages associated with solid-phase reactors as opposed to their homogeneous (solution) counterparts: (1) reuse of the immobilized reagent for subsequent analysis;[38,250,251] (2) enhanced stability and activity of the reagent when immobilized to a solid-support;[252–254] and (3) simplified on-line processing of the sample in fluidic systems as well as easier separation of the reaction products from the catalytic enzyme or removal of the interfering components from the selected target.

The shortcomings associated with many solid-phase reactors are two-fold. First, diffusional kinetic barriers are produced by immobilizing the reagents to a solid support. Basically, for a reaction to occur, the target must diffuse to the surface. For flow-through solid-phase bioreactors, the conversion efficiency can be calculated from $A_{\mathrm{L}}=[A]_{\mathrm{o}}\mathrm{e}^{-\left[\frac{14.43D_{\mathrm{A}}l}{\nu d^2}\right]}$ where A_{L} the concentration of the target molecule leaving the reactor channel, $[A]_{\mathrm{o}}$ is the concentration of the target at the entrance of the solid-phase reactor channel, D_{A} is the target diffusion coefficient, l is the length of the reactor, ν is the linear velocity through the reactor and d is the diameter of the reactor channel. A graphical representation of the predictions from this equation is shown in Fig. 14 for a reactor consisting of an immobilized enzyme converting a solution-target into a product. As can be seen from this figure, reducing the reactor dimensions has a profound impact on the efficiency of conversion of the chemical reactant into product during travel through the reactor, even for targets that have relatively small diffusion coefficients. Therefore, nanofluidics is particularly attractive as a container for performing flow-through solid-phase reactions because the diffusional barrier is minimal compared to the chemical kinetic barrier imposed by the immobilized reagent.

Examples of nano-scale reactors in polymer substrates using horizontal nanochannels or nanoslits have not been documented in the literature to-date. However, polymer-based microchannels populated with ultra-high aspect ratio nanopillars containing immobilized trypsin (proteolytic enzyme that cleaves peptide bonds at arginine and lysine residues) have been reported.[255,256] In this work, microchannels and the nanopillar supports were fabricated in PMMA using hot embossing to make the fluidic network and sacrificial template with anodized aluminium oxide pores to fabricate the nanopillars (see Fig. 15). The

pillars were 150 nm in diameter with a height of 100 μm (aspect ratio = 667). Trypsin was covalently attached to the pillars by exposing the PMMA to UV radiation, which induced photo-oxidation reactions generating surface-confined carboxylic acids.[45] The enzyme could then be attached through primary amine groups to the surface *via* an amide bond. The nano-reactor performance was compared to an open channel (50 μm wide). Lineweaver–Burk analysis was carried out to evaluate V_{max} (the velocity of the reaction when the active sites of the enzyme were saturated with substrate). This analysis yielded values for V_{max} of 5.02 and 51.8 mM min^{-1} for the immobilized trypsin in the open channel versus the nanopillar PMMA channel, respectively.

5. Conclusions

Nanofluidics is attracting significant attention due to the unique phenomena afforded through the use of confined environments on the molecular-scale. For example, applications in DNA elongation have generated some exciting new strategies for mapping sequence variations. In addition, new strategies are evolving that use nanochannels and/or nanoslits to assist in the process of securing primary structural information from nucleic acids at unprecedented throughput and cost (*i.e.*, DNA/RNA sequencing). Other compelling applications for nanofluidics include analyte preconcentration due to concentration polarization effects and nano-scale separations. As with any new technology, nanofluidics implementation in a broad range of application areas will depend on the accessibility of the technology to a wide user base as well as facile transitioning into the private sector, which will depend on the ability to mass produce the technology at low-cost and with high fidelity. The predominant fabrication mode for devices appropriate for nanofluidics currently uses predominately glass-like substrates with the prerequisite structures produced *via* EBL or FIB patterning directly into the device. Unfortunately, the low throughput and high cost of producing nanostructures using this modality can be prohibitive to realize effective expansion of this exciting technology area.

Polymer nanofluidics, using either elastomeric or thermo-plastic materials, is an attractive alternative to glass-based nanofluidics. The compelling attribute of polymer nanofluidics is the ability to generate devices in a high production mode using nano-replication techniques. This basically eliminates the need to reproduce the desired nanostructures directly into the device; a master or stamp containing the desired structures can be used to produce many replicas without requiring EBL or FIB patterning of each device. In addition, once the master or stamp is made, it can be used to produce devices in a variety of material to suite the particular application need. Many of these fabrication strategies can employ hierarchical protocols, in which the microstructures can be integrated with the nanostructures onto the same master to produce a mixed-scale device spanning from the mm to nm size-domain. In the case of elastomers, the low Young's modulus of these materials makes them attractive for altering the size-scale of the preformed nanochannels/nanoslits to accommodate or expand upon the device's capability. For example, entropic barriers typically make it difficult to load DNAs into cross-sectional channels with dimensions smaller than the persistence length of the double-stranded DNA (~50 nm). To facilitate loading, sub-micron channels can be formed in PDMS and then, once loaded with the DNA, the substrate can be stretched to reduce the size of the nanochannel to enhance the degree of elongation.

In spite of their diverse and efficient fabrication protocols that can be employed to generate nanofluidic devices, there are some challenges when using polymers as substrate materials, the most notable one being the relatively small Young's modulus associated with these materials, which makes cover plate assembly to the patterned substrate difficult due to cover plate collapse and/or nanostructure deformation using either thermal or chemical bonding to enclose the fluidic network. In conjunction with this is the buckling of the substrate that can result when there is a large mismatch between the thermal expansion coefficient of the molding tool and the work piece. This mismatch can make cover plate assembly difficult as well. An additional issue that must be addressed is the surface roughness of molded nanostructures, which can result from roughness in the master itself or additional roughness that is produced during demolding when NIL is used to produce the desired structures. Direct patterning of nanostructures into the substrate as is done for glass-based devices does not possess this problem. Some of these issues can be addressed by employing anti-sticking coatings onto the molding tool to alter the surface energy.

Another appealing attribute of polymers for nanofluidic applications is the diverse range of surface properties that can be generated by simply selecting the appropriate polymer substrate for the device. In many cases, proper selection of the polymer substrate can produce a nanofluidic channel that is compatible for the intended application, such as nanochromatography where solute/wall interactions are critical for producing the appropriate separation results. In addition, polymer-based devices can be operated at extreme pH conditions as opposed to glass-based devices. Glass substrates can be etched in high pH solutions, which may effectively enlarge the nanochannel during device operation, compromising the operational performance. Polymer substrates tend to be more tolerant of high pH solutions. However, polymers can be less tolerant of many organic solvents compared to glass, which could limit their use in applications such as fLC. Even when surface modification is necessary, the polymer support can be used directly or modified to create functional scaffolds to allow for the covalent attachment of the necessary material. For example, UV or plasma oxidation of most polymers produces a surface rich in oxygen-containing functionalities, such as alcohols and carbonyls. These surface modification protocols have also been used to assist in the thermal assembly of the fluidic device as well as altering the surface charge density, which can impact the performance of the device for preconcentration applications or altering the magnitude of the EOF as well as mitigating potential solute/wall electrostatic interactions. However, while there is a plethora of surface modification strategies that can be used with different polymeric materials and these have been well documented in the case of polymer microfluidics, their implementation in nanofluidics is not so well documented at the current time.

Applications of nanofluidics in biology and chemistry have been demonstrated using predominately glass-based devices and the list of potential applications continues to grow. Many of these applications can be envisioned to effectively translate over well to polymer nanofluidics, but wait to be demonstrated as the device fabrication/assembly protocols continue to be documented and optimized. The most noted application area for polymer nanofluidics to-date has been in the stretching/ elongation of DNA with some interesting results including surface energy effects on DNA stretching as well as the modulation of the channel dimensions through the application of an external load. It will be interesting in the

future to compare and contrast the performance metrics of polymer nanofluidic devices to their glass counterparts in different applications.

Acknowledgements

This work was partially sponsored by WCU (World Class University) program (R32-2008-000-20054-0) and the National Institutes of Health (NIH). One author (Park) would like to thank the Center for Nanoscale Mechatronics & Manufacturing (CNMM), one of the 21st Century Frontier Research programs from the Ministry of Science and Technology, Korea, for partial support of this work.

Biography

Rattikan Chantiwas

Rattikan Chantiwas is currently a faculty member of the Department of Chemistry and the Center of Excellence for Innovation in Chemistry, Faculty of Science, Mahidol University in Bangkok, Thailand. She obtained her BS and MS from Mahidol University and her PhD in Chemistry from Chiang Mai University in 2003 under the Royal Golden Jubilee Scholarship from the Thailand Research Fund. She was a postdoctoral researcher in Prof Steven A. Soper's laboratory at Louisiana State University, where she was also a WCU research scholar at UNIST, Korea. Her research interests focus on microfluidic devices, fabrication and applications for bioanalytical chemistry.

Sunggook Park

Sunggook Park is an associate professor of Mechanical Engineering and a faculty member of the Center for Bio-Modular Multiscale Systems at Louisiana State University and leading the Nanosystems Group. He received his BS and MS in Chemical Engineering from Yonsei University, Korea, and a PhD in Physics at Technical University Chemnitz, Germany. He was a post-doctoral researcher at the Laboratory for Micro- and Nanotechnology in Paul Scherrer Institute, Switzerland, where he gained expertise in nanofabrication and nanoimprint lithography. His current research interests include nanomolding, 3-D

nanofabrication, nanofluidic devices and transport for bioapplications. He received a National Science Foundation's Faculty Early Career Award in 2007.

Steven A. Soper

Steven A. Soper is the William L. & Patricia Senn Professor of Chemistry, Professor of Mechanical Engineering and Director of the Center for Bio-Modular Multiscale Systems at Louisiana State University. He is also a WCU Scholar at UNIST, Korea, as well as a Fellow of the AAAS, Royal Society of Chemistry and Society for Applied Spectroscopy. He received his PhD in 1989 from the University of Kansas and then a post-doctoral fellowship at Los Alamos National Laboratory. His research interests focus on polymer micro-/nanofluidics for applications ranging from in vitro diagnostics to basic biological discovery. He has published >250 manuscripts, particularly in the areas of single-molecule detection and micro/nanofluidics.

Shuichi Takayama and Byoung Choul Kim

Byoung Choul Kim is a PhD Candidate in Department of Biomedical Engineering at the University of Michigan under the supervision of Dr Takayama. His research interests focus on nanofluidics and genomic analysis.

Shuichi Takayama is a Professor in the Department of Biomedical Engineering and the Macromolecular Science and Engineering Program at the University of Michigan. He is also a WCU Visiting Professor at Ulsan National Institute of Science and Technology in Korea. His research interests include nanofluidics and genomic analysis, microfluidics and cell/tissue engineering.

Vijaya Sunkara, Yoon-Kyoung Cho and Hyundoo Hwang

Vijaya Sunkara is a postdoctoral researcher at UNIST. She obtained her BSc in Chemistry & Biology and MSc in Organic Chemistry from Osmania University, Hyderabad, India, in 1995 and 1998, respectively. She received her PhD in Organic Chemistry from Jawaharlal

Nehru Technological University (JNTU), India, in 2004. She worked as a postdoctoral researcher (2004–2006), and a research scientist (2006–2009) at Pohang University of Science & Technology (POSTECH) and NSBPOSTECH, Korea, respectively, where she was involved in the development of nano-scale controlled surfaces for DNA microarrays. Her current research focuses on surface modification of various materials like silicon, polymers and carbon for integrated devices.

Hyundoo Hwang is a postdoctoral researcher at UNIST. He received his BS, MS, and PhD in bio- and brain engineering from the Korea Advanced Institute of Science and Technology (KAIST) in 2006, 2007, and 2010, respectively. He is interested in optoelectronic nano/microfluidic platforms for clinical diagnostics, cell biology, and environmental science. He received a National Science Scholarship (2003–2006) from the Korea Science and Engineering Foundation, and a PhD Scholarship Award (2008–2010) from the Seoam Scholarship Foundation in Korea.

Yoon-Kyoung Cho is currently an associate professor at UNIST. She is also the director of the World Class University (WCU) program, “Nano Science and Technology for Advanced Diagnostics and Personalized Medicine”, at UNIST. She received her PhD in Materials Science and Engineering from the University of Illinois at Urbana-Champaign in 1999, having obtained her MS and BS in Chemical Engineering from POSTECH in 1994 and in 1992, respectively. Before joining UNIST, she worked at Samsung Advanced Institute of Technology (SAIT) for 9 years focused on the development of lab-on-a-chip devices for biomedical applications. Her current research interests include novel nano/microfluidic devices for advanced diagnostics, environmental monitoring and cell biology.

Abbreviations

A_L	concentration of the target molecule leaving the micro-reactor channel
$[A]_o$	concentration of the target at the entrance of the micro-reactor
D_A	target diffusion coefficient
E_1	plane-strain modulus of PDMS oxidized layer
E_2	Young's modulus of unoxidized PDMS
E	Young's modulus
E′	4/3*E* and denotes plane-strain modulus
E_V	applied electric field
I_s	ionic strength
T_g	glass transition temperature
T_m	melting temperature
γ_W	work of adhesion between stamp and substrate
2*a*	punch spacing

h_P	punch height
$2w$	punch width
γ	surface energy of nanochannel walls
c_c	closure distance
C_i	electrolyte concentration
d	diameter of the reactor channel
σ_a	remote applied compressive stress
h	height of nanochannel
h_f	thickness of polymer oxidized layer
l	length of the reactor
V_{max}	velocity of reaction when active sites of enzyme are saturated with substrate
$2a$	base length of channel cross section
σ_s	surface charge density
q_i	net charge on ion
z_i	valency of ion
e	electron charge
ψ	potential distribution in EDL of charged interface
κ	Debye–Hückel parameter
z	surface normal direction
λ_D	Debye length
v_{eo}	electroosmotic velocity
ε	relative dielectric permittivity
ε_o	vacuum permittivity
ζ	zeta potential
μ	dynamic viscosity of electrolyte solution
ν	linear velocity of target through reactor
σ_Y	yield strength
ΔT	$T - T_g$, T = molding temperature
ΔP_L	capillary or Laplace pressure
r	capillary radius
θ_C	water contact angle
γ	surface tension of the liquid in air

k	permeability
ΔP_E	pressure drop along the nanochannels
l	length (nanochannel)
A	cross-sectional area (nanochannel)
h	microchannel height
w	microchannel width
L	liquid front position
t	time
Q	flow rate
R	hydraulic radius
η	solution viscosity
C_g	shape factor of the channel/slit

References

1. Abgrall P, Nguyen NT. Anal. Chem. 2008; 80:2326–2341. [PubMed: 18321133]
2. Bohn PW. Annu. Rev. Anal. Chem. 2009; 2:279–296.
3. Eijkel JCT, van den Berg A. Microfluid. Nanofluid. 2005; 1:249–267.
4. Kovarick ML, Jacobson SC. Anal. Chem. 2009; 81:7133–7140. [PubMed: 19663470]
5. Daiguji H. Chem. Soc. Rev. 2010; 39:901–911. [PubMed: 20179813]
6. Cheng L-J, Guo LJ. Chem. Soc. Rev. 2010; 39:923–938. [PubMed: 20179815]
7. Kim SJ, Song Y-A, Han J. Chem. Soc. Rev. 2010; 39:912–922. [PubMed: 20179814]
8. Zangle TA, Mani A, Santiago JG. Chem. Soc. Rev. 2010; 39:1014–1035. [PubMed: 20179822]
9. van Honschoten JW, Brunets N, Tas NR. Chem. Soc. Rev. 2010; 39:1096–1114. [PubMed: 20179827]
10. Siwy ZS, Howorka S. Chem. Soc. Rev. 2010; 39:1115–1132. [PubMed: 20179828]
11. Levy SL, Craighead HG. Chem. Soc. Rev. 2010; 39:1133–1152. [PubMed: 20179829]
12. Persson F, Tegenfeldt JO. Chem. Soc. Rev. 2010; 39:985–999. [PubMed: 20179820]
13. Keyser UF, van Dorp S, Lemay SG. Chem. Soc. Rev. 2010; 39:939–947. [PubMed: 20179816]
14. Piruska A, Gong M, Sweedler JV, Bohn PW. Chem. Soc. Rev. 2010; 39:1060–1072. [PubMed: 20179825]
15. Tsukahara T, Mawatari K, Kitamori T. Chem. Soc. Rev. 2010; 39:1000–1013. [PubMed: 20179821]
16. Jo K, Dhingra DM, Odijk T, de Pablo JJ, Graham MD, Runnheim R, Forrest D, Schwartz DC. Proc. Natl. Acad. Sci. U. S. A. 2007; 104:2673–2678. [PubMed: 17296933]
17. Liang XG, Chou SY. Nano Lett. 2008; 8:1472–1476. [PubMed: 18416580]
18. Rotting O, Ropke W, Becker H, Gartner C. Microsyst. Technol. 2002; 8:32–36.
19. Soper SA, Ford SM, Qi S, McCarley RL, Kelly K, Murphy MC. Anal. Chem. 2000; 72:642A–651A.
20. Baker LA, Choi Y, Martin CR. Curr. Nanosci. 2006; 2:243–255.
21. Spohr R. Radiat. Meas. 2005; 40:191–202.
22. Ford SM, Davies J, Kar B, Qi SD, McWhorter S, Soper SA, Malek CK. J. Biomech. Eng. 1999; 121:13–21. [PubMed: 10080084]

23. Ford SM, Kar B, McWhorter S, Davies J, Soper SA, Klopf M, Calderon G, Saile V. J. Microcolumn Sep. 1998; 10:413–422.
24. Soper SA, Henry AC, Vaidya B, Galloway M, Wabuyele M, McCarley RL. Anal. Chim. Acta. 2002; 470:87–99.
25. Bai YL, Koh CG, Boreman M, Juang YJ, Tang IC, Lee LJ, Yang ST. Langmuir. 2006; 22:9458–9467. [PubMed: 17042569]
26. Cretich M, Sedini V, Damin F, Di Carlo G, Oldani C, Chiari M. Sens. Actuators, B. 2008; 132:258–264.
27. Goddard JM, Hotchkiss JH. Prog. Polym. Sci. 2007; 32:698–725.
28. Situma C, Wang Y, Hupert M, Barany F, McCarley RL, Soper SA. Anal. Biochem. 2005; 340:123–135. [PubMed: 15802138]
29. Soper SA, Hashimoto M, Situma C, Murphy MC, McCarley RL, Cheng YW, Barany F. Methods. 2005; 37:103–113. [PubMed: 16199178]
30. Wang Y, Vaidya B, Farquar HD, Stryjewski W, Hammer RP, McCarley RL, Soper SA, Cheng YW, Barany F. Anal. Chem. 2003; 75:1130–1140. [PubMed: 12641233]
31. Wong I, Ho CM. Microfluid. Nanofluid. 2009; 7:291–306. [PubMed: 20357909]
32. Zhou JW, Ellis AV, Voelcker NH. Electrophoresis. 2010; 31:2–16. [PubMed: 20039289]
33. Kochkodan VM, Hilal N, Goncharuk VV, Al-Khatib L, Levadna TI. Colloid J. 2006; 68:267–273.
34. Lee JA, McCarthy TJ. Macromolecules. 2007; 40:3965–3969.
35. Liu SX, Kim JT, Kim S. J. Food Sci. 2008; 73:E143–E150. [PubMed: 18387109]
36. Wu YZ, Coyer SR, Ma HW, Garcia AJ. Acta Biomater. 2010; 6:2898–2902. [PubMed: 20176151]
37. Xu Y, Takai M, Ishihara K. Ann. Biomed. Eng. 2010; 38:1938–1953. [PubMed: 20358288]
38. Davidson YY, Soper SA, Margolis S, Sander LC. J. Sep. Sci. 2001; 24:10–16.
39. Lee J, Soper SA, Murray KK. Analyst. 2009; 134:2426–2433. [PubMed: 19918612]
40. Witek MA, Hupert ML, Park DSW, Fears K, Murphy MC, Soper SA. Anal. Chem. 2008; 80:3483–3491. [PubMed: 18355091]
41. Witek MA, Llopis S, Wheatley A, McCarley R, Soper SA. Nucleic Acids Res. 2006; 34:e74. [PubMed: 16757572]
42. Xu YC, Vaidya B, Patel AB, Ford SM, McCarley RL, Soper SA. Anal. Chem. 2003; 75:2975–2984. [PubMed: 12964741]
43. Chan CM, Ko TM, Hiraoka H. Surf. Sci. Rep. 1996; 24:3–54.
44. Kim YJ, Taniguchi Y, Murase K, Taguchi Y, Sugimura H. Appl. Surf. Sci. 2009; 255:3648–3654.
45. McCarley RL, Vaidya B, Wei SY, Smith AF, Patel AB, Feng J, Murphy MC, Soper SA. J. Am. Chem. Soc. 2006; 127:842–843. [PubMed: 15656615]
46. Borcia C, Borcia G, Dumitrascu N. J. Optoelectron. Adv. Mater. 2008; 10:675–679.
47. Duffy DC, McDonald JC, Schueller OJA, Whitesides GM. Anal. Chem. 1998; 70:4974–4984. [PubMed: 21644679]
48. Martin IT, Dressen B, Boggs M, Liu Y, Henry CS, Fisher ER. Plasma Processes Polym. 2007; 4:414–424.
49. Xu F, Datta P, Wang H, Gurung S, Hashimoto M, Wei S, Goettert J, McCarley RL, Soper SA. Anal. Chem. 2007; 79:9007–9013. [PubMed: 17949012]
50. Yang SJ, Yin H. Plasma Chem. Plasma Process. 2007; 27:23–33.
51. Ye HK, Gu ZY, Gracias DH. Langmuir. 2006; 22:1863–1868. [PubMed: 16460119]
52. Choi WK. Surf. Coat. Technol. 2007; 201:8099–8104.
53. Ginn BT, Steinbock O. Langmuir. 2003; 19:8117–8118.
54. Sun XF, Liu JK, Lee ML. Electrophoresis. 2008; 29:2760–2767. [PubMed: 18615784]
55. Barker SLR, Ross D, Tarlov MJ, Gaitan M, Locascio LE. Anal. Chem. 2000; 72:5925–5929. [PubMed: 11140758]
56. Barker SLR, Tarlov MJ, Canavan H, Hickman JJ, Locascio LE. Anal. Chem. 2000; 72:4899–4903. [PubMed: 11055706]
57. Chen W, McCarthy TJ. Macromolecules. 1997; 30:78–86.

58. Phuvanartnuruks V, McCarthy TJ. Macromolecules. 1998; 31:1906–1914.
59. Chantiwas R, Hupert ML, Pullagurla S, Balamurugan S, Lopez JT, Park S, Datta P, Goettert J, Cho YK, Soper SA. Lab Chip. 2010; 10:3255–3264. [PubMed: 20938506]
60. Tennico YH, Koesdjojo MT, Kondo S, Mandrell DT, Remcho VT. Sens. Actuators, B. 2010; 143:799–804.
61. Tsao CW, DeVoe DL. Microfluid. Nanofluid. 2009; 6:1–16.
62. Wei SY, Vaidya B, Patel AB, Soper SA, McCarley RL. J. Phys. Chem. B. 2005; 109:16988–16996. [PubMed: 16853163]
63. Heckele M, Schomburg WK. J. Micromech. Microeng. 2004; 14:R1–R14.
64. Chou SY, Krauss PR, Renstrom PJ. Appl. Phys. Lett. 1995; 67:3114–3116.
65. Chou SY, Krauss PR, Renstrom PJ. Science. 1996; 272:85–87.
66. Al-Assaad RM, Regonda S, Tao L, Pang SW, Hu WW. J. Vac. Sci. Technol., B. 2007; 25:2396–2401.
67. Dupaix RB, Cash W. Polym. Eng. Sci. 2009; 49:531–543.
68. Heyderman LJ, Schift H, David C, Gobrecht J, Schweizer T. Microelectron. Eng. 2000; 54:229–245.
69. Hirai Y, Fujiwara M, Okuno T, Tanaka Y, Endo M, Irie S, Nakagawa K, Sasago M. J. Vac. Sci. Technol., B. 2001; 19:2811–2815.
70. Hirai Y, Konishi T, Yoshikawa T, Yoshida S. J. Vac. Sci. Technol., B. 2004; 22:3288–3293.
71. Jeong JH, Choi YS, Shin YJ, Lee JJ, Park KT, Lee ES, Lee SR. Fibers Polym. 2002; 3:113–119.
72. Mohamed K, Alkaisi MM, Smaill J. Curr. Appl. Phys. 2006; 6:486–490.
73. Rowland HD, King WP. J. Micromech. Microeng. 2004; 14:1625–1632.
74. Rowland HD, King WP, Sun AC, Schunk PR. J. Vac. Sci. Technol., B. 2005; 23:2958–2962.
75. Scheer HC, Schulz H. Microelectron. Eng. 2001; 56:311–332.
76. Schift H, David C, Gabriel M, Gobrecht J, Heyderman LJ, Kaiser W, Koppel S, Scandella L. Microelectron. Eng. 2000; 53:171–174.
77. Schift H, David C, Gobrecht J, D'Amore A, Simoneta D, Kaiser W, Gabriel M. J. Vac. Sci. Technol., B. 2000; 18:3564–3568.
78. Schift H, Heyderman LJ, Gobrecht J. Chimia. 2002; 56:543–546.
79. Schift H, Heyderman LJ, Maur MAD, Gobrecht J. Nanotechnology. 2001; 12:173–177.
80. Schift H, Park S, Gobrecht J. J. Photopolym. Sci. Technol. 2003; 16:435–438.
81. Takagi H, Takahashi M, Maeda R, Onishi Y, Iriye Y, Iwasaki T, Hirai Y. Microelectron. Eng. 2008; 85:902–906.
82. Woo YS, Lee DE, Il Lee W. Tribol. Lett. 2009; 36:209–222.
83. Young WB. Microelectron. Eng. 2005; 77:405–411.
84. Acikgoz C, Hempenius MA, Vancso GJ, Huskens J. Nanotechnology. 2009; 20:135304. [PubMed: 19420495]
85. Choi P, Fu PF, Guo LJ. Adv. Funct. Mater. 2007; 17:65–70.
86. Houle FA, Guyer E, Miller DC, Dauskardt R. J. Vac. Sci. Technol., B. 2007; 25:1179–1185.
87. Mekaru H, Takahashi M. Jpn. J. Appl. Phys. 2008; 47:5178–5184.
88. Peroz C, Chauveau V, Barthel E, Sondergard E. Adv. Mater. 2009; 21:555–+. [PubMed: 21161980]
89. Pfeiffer K, Bleidiessel G, Gruetzner G, Schulz H, Hoffmann T, Scheer HC, Torres CMS, Ahopelto J. Microelectron. Eng. 1999; 46:431–434.
90. Pfeiffer K, Reuther F, Fink M, Gruetzner G, Carlberg P, Maximov I, Montelius L, Seekamp J, Zankovych S, Sotomayor-Torres CM, Schulz H, Scheer HC. Microelectron. Eng. 2003; 67–68:266–273.
91. Schuster C, Reuther F, Kolander A, Gruetzner G. Microelectron. Eng. 2009; 86:722–725.
92. Taniguchi J, Kawasaki T, Tokano Y, Kogo Y, Miyamoto I, Komuro M, Hiroshima H, Sakai N, Tada K. Jpn. J. Appl. Phys., Part 1. 2002; 41:4194–4197.

93. Toralla KP, De Girolamo J, Truffier-Boutry D, Gourgon C, Zelsmann M. Microelectron. Eng. 2009; 86:779–782.
94. Yan YH, Chan-Park MB, Ching WC, Yue CY. Appl. Surf. Sci. 2005; 249:332–339.
95. Zelsmann M, Toralla K, De Girolamo J, Boutry D, Gourgon C. J. Vac. Sci. Technol., B. 2008; 26:2430–2433.
96. Fuchs A, Vratzov B, Wahlbrink T, Georgiev Y, Kurz H. J. Vac. Sci. Technol., B. 2004; 22:3242–3245.
97. Kong YP, Tan L, Pang SW, Yee AF. J. Vac. Sci. Technol., A. 2004; 22:1873–1878.
98. Li NH, Wu W, Chou SY. Nano Lett. 2006; 6:2626–2629. [PubMed: 17090103]
99. Pagliara S, Persano L, Camposeo A, Cingolani R, Pisignano D. Nanotechnology. 2007; 18:175302.
100. Picciotto C, Gao J, Hoarau E, Wu W. Appl. Phys. A. 2005; 80:1287–1299.
101. Picciotto C, Gao J, Hoarau E, Wu W, Jackson W, Tong WM. J. Vac. Sci. Technol., B. 2005; 23:3047–3051.
102. Picciotto C, Gao J, Yu Z, Wu W. Nanotechnology. 2009; 20:255304. [PubMed: 19487804]
103. Stewart DR, Gibson G, Jung GY, Wu W, Straznicky J, Tong W, Li Z, Williams RS. Nanotechnology. 2007; 18:415201.
104. Wu W, Tong WM, Bartman J, Chen YF, Walmsley R, Yu ZN, Xia QF, Park I, Picciotto C, Gao J, Wang SY, Morecroft D, Yang J, Berggren KK, Williams RS. Nano Lett. 2008; 8:3865–3869. [PubMed: 18837563]
105. Ahn SW, Lee KD, Kim JS, Kim SH, Park JD, Lee SH, Yoon PW. Nanotechnology. 2005; 16:1874–1877.
106. Ansari K, van Kan JA, Bettiol AA, Watt F. Appl. Phys. Lett. 2004; 85:476–478.
107. Chen XZ, Li HY. Chin. Phys. Lett. 2007; 24:2830–2832.
108. Gadegaard N, McCloy D. Microelectron. Eng. 2007; 84:2785–2789.
109. Grego S, Huffman A, Lueck M, Stoner BR, Lannon J. Microelectron. Eng. 2010; 87:1846–1851.
110. Haatainen T, Makela T, Ahopelto J, Kawaguchi Y. Microelectron. Eng. 2009; 86:2293–2296.
111. Hong SH, Lee JH, Lee H. Microelectron. Eng. 2007; 84:977–979.
112. Hong SH, Yang K, Lee H. Eco-Materials Processing & Design VII. 2006; 510–511:462–465.
113. Kehagias N, Reboud V, De Girolamo J, Chouiki M, Zelsmann M, Boussey J, Torres CMS. Microelectron. Eng. 2009; 86:776–778.
114. Ki KD, Jeong JH, Park SH, Choi DG, Choi JH, Lee ES. Microelectron. Eng. 2009; 86:1983–1988.
115. Kim JS, Lee KD, Ahn SW, Kim SH, Park JD, Lee SE, Yoon SS. J. Korean Phys. Soc. 2004; 45:S890–S892.
116. Kim TS, Kim SM, Song SS, Kim EU, Lee K, Kim KS, Jung GY. J. Nanosci. Nanotechnol. 2008; 8:5275–5278. [PubMed: 19198437]
117. Park IS, Kim JS, Na SH, Lim SK, Oh YS, Suh SJ. Microelectron. Eng. 2010; 87:1707–1710.
118. Park S, Schift H, Solak HH, Gobrecht J. J. Vac. Sci. Technol., B. 2004; 22:3246–3250.
119. Pfeiffer K, Fink M, Ahrens G, Gruetzner G, Reuther F, Seekamp J, Zankovych S, Torres CMS, Maximov I, Beck M, Graczyk M, Montelius L, Schulz H, Scheer HC, Steingrueber F. Microelectron. Eng. 2002; 61–62:393–398.
120. Schift H, Spreu C, Saidani M, Bednarzik M, Gobrecht J, Klukowska A, Reuther F, Gruetzner G, Solak HH. J. Vac. Sci. Technol., B. 2009; 27:2846–2849.
121. Viheriala J, Rytkonen T, Niemi T, Pessa M. Nanotechnology. 2008; 19:015302. [PubMed: 21730528]
122. Zhao YP, Berenschot E, Jansen H, Tas N, Huskens J, Elwenspoek M. Microelectron. Eng. 2009; 86:832–835.
123. Kim WS, Jin JH, Bae BS. Nanotechnology. 2006; 17:1212–1216.
124. Park S, Schift H, Padeste C, Schnyder B, Kotz R, Gobrecht J. Microelectron. Eng. 2004; 73–74:196–201.
125. Schift H, Saxer S, Park S, Padeste C, Pieles U, Gobrecht J. Nanotechnology. 2005; 16:S171–S175.

126. Sun HW, Liu JQ, Gu P, Chen D. Appl. Surf. Sci. 2008; 254:2955–2959.
127. Tallal J, Gordon M, Berton K, Charley AL, Peyrade D. Microelectron. Eng. 2006; 83:851–854.
128. Truffier-Boutry D, Beaurain A, Galand R, Pelissier B, Boussey J, Zelsmann M. Microelectron. Eng. 2010; 87:122–124.
129. Truffier-Boutry D, Galand R, Beaurain A, Francone A, Pelissier B, Zelsmann M, Boussey J. Microelectron. Eng. 2009; 86:669–672.
130. Austin MD, Ge HX, Wu W, Li MT, Yu ZN, Wasserman D, Lyon SA, Chou SY. Appl. Phys. Lett. 2004; 84:5299–5301.
131. Chou SY, Krauss PR. Microelectron. Eng. 1997; 35:237–240.
132. Chou SY, Krauss PR, Renstrom PJ. J. Vac. Sci. Technol., B. 1996; 14:4129–4133.
133. Gates BD, Whitesides GM. J. Am. Chem. Soc. 2003; 125:14986–14987. [PubMed: 14653723]
134. Guo LJ. J. Phys. D. 2004; 37:R123–R141.
135. Guo LJ. Adv. Mater. 2007; 19:495–513.
136. Schift H. J. Vac. Sci. Technol., B. 2008; 26:458–480.
137. Sotomayor Torres, CM., editor. Alternative lithography: unleashing the potentials of nanotechnology. Kluwer; Boston: 2003.
138. Torres CMS, Zankovych S, Seekamp J, Kam AP, Cedeno CC, Hoffmann T, Ahopelto J, Reuther F, Pfeiffer K, Bleidiessel G, Gruetzner G, Maximov MV, Heidari B. Mater. Sci. Eng., C. 2003; 23:23–31.
139. Zankovych S, Hoffmann T, Seekamp J, Bruch JU, Torres CMS. Nanotechnology. 2001; 12:91–95.
140. Park S, Song ZC, Brumfield L, Amirsadeghi A, Lee J. Appl. Phys. A: Mater. Sci. Process. 2009; 97:395–402.
141. Chan-Park MB, Yan YH, Neo WK, Zhou WX, Zhang J, Yue CY. Langmuir. 2003; 19:4371–4380.
142. Kim JY, Choi DG, Jeong JH, Lee ES. Appl. Surf. Sci. 2008; 254:4793–4796.
143. Yang R, Soper SA, Wang WJ. Sens. Actuators, A. 2007; 135:625–636.
144. Fillman RW, Krchnavek RR. J. Vac. Sci. Technol., B. 2009; 27:2869–2872.
145. Schvartzman M, Mathur A, Kang Y, Jahnes C, Hone J, Wind SJ. J. Vac. Sci. Technol., B. 2008; 26:2394–2398.
146. Tao L, Ramachandran S, Nelson CT, Lin M, Overzet LJ, Goeckner M, Lee G, Willson CG, Wu W, Hu W. Nanotechnology. 2008; 19:105302. [PubMed: 21817695]
147. Yamada N, Nakamatsu KI, Kanda K, Haruyama Y, Matsui S. Jpn. J. Appl. Phys., Part 1. 2007; 46:6373–6374.
148. Guo YH, Liu G, Xiong Y, Tian YC. J. Micromech. Microeng. 2007; 17:9–19.
149. Song Z, Choi J, You BH, Lee J, Park S. J. Vac. Sci. Technol., B. 2008; 26:598–605.
150. Song ZC, You BH, Lee J, Park S. Microsyst. Technol. 2008; 14:1593–1597.
151. Worgull M, Heckele M, Hetu JF, Kabanemi KK. J. Microlithogr., Microfabr., Microsyst. 2006; 5:13.
152. Worgull M, Heckele M, Schomburg WK. Microsyst. Technol. 2005; 12:110–115.
153. Abad E, Merino S, Retolaza A, Juarros A. Microelectron. Eng. 2008; 85:818–821.
154. Bilenberg B, Jacobsen S, Schmidt MS, Skjolding LHD, Shi P, Boggild P, Tegenfeldt JO, Kristensen A. Microelectron. Eng. 2006; 83:1609–1612.
155. Carlberg P, Montelius L, Tegenfeldt J. Microelectron. Eng. 2008; 85:210–213.
156. Tegenfeldt JO, Cao H, Reisner WW, Prinz C, Austin RH, Chou SY, Cox EC, Sturm JC. Biophys. J. 2004; 86:596A–596A.
157. Tegenfeldt JO, Prinz C, Cao H, Chou S, Reisner WW, Riehn R, Wang YM, Cox EC, Sturm JC, Silberzan P, Austin RH. Proc. Natl. Acad. Sci. U. S. A. 2004; 101:10979–10983. [PubMed: 15252203]
158. Tegenfeldt JO, Prinz C, Cao H, Huang RL, Austin RH, Chou SY, Cox EC, Sturm JC. Anal. Bioanal. Chem. 2004; 378:1678–1692. [PubMed: 15007591]

159. Thamdrup LH, Klukowska A, Kristensen A. Nanotechnology. 2008; 19:125301. [PubMed: 21817722]
160. Whitesides GM, Ostuni E, Takayama S, Jiang X. Annu. Rev. Biomed. Eng. 2001; 3:335–373. [PubMed: 11447067]
161. Kuo T, Cannon Jr D, Chen Y, Tulock J, Shannon M, Sweedler J, Bohn P. Science. 1993; 261:895–897. [PubMed: 17783736]
162. Hui C, Jagota A, Lin Y, Kramer E. Langmuir. 2002; 18:1394–1407.
163. Huang Y, Zhou W, Hsia K, Menard E, Park J, Rogers J, Alleyne A. Langmuir. 2005; 21:8058–8068. [PubMed: 16089420]
164. Zhou W, Huang Y, Menard E, Aluru N, Rogers J, Alleyne A. Appl. Phys. Lett. 2005; 87:251925.
165. Huh D, Mills KL, Zhu XY, Burns MA, Thouless MD, Takayama S. Nat. Mater. 2007; 6:424–428. [PubMed: 17486084]
166. Mills K, Huh D, Takayama S, Thouless M. Lab Chip. 2010; 10:1627–1630. [PubMed: 20517560]
167. Bowden N, Huck W, Paul K, Whitesides G. Appl. Phys. Lett. 1999; 75:2557.
168. Efimenko K, Rackaitis M, Manias E, Vaziri A, Mahadevan L, Genzer J. Nat. Mater. 2005; 4:293–297. [PubMed: 15750598]
169. Chung S, Lee JH, Moon M-W, Han J, Kamm RD. Adv. Mater. 2008; 20:3011–3016.
170. Bellan L, Strychalski E, Craighead H. J. Vac. Sci. Technol., B. 2008; 26:1728.
171. Park K, Lee S, Takama N, Fujii T, Kim B. Microelectron. Eng. 2009; 86:1385–1388.
172. Park S-M, Huh YS, Craighead HG, Erickson D. Proc. Natl. Acad. Sci. U. S. A. 2009; 106:15549–15554. [PubMed: 19717418]
173. Chang THP, Mankos M, Lee KY, Muray LP. Microelectron. Eng. 2001; 57–58:117–135.
174. Chang THP, Thomson MGR, Kratschmer E, Kim HS, Yu ML, Lee KY, Rishton SA, Hussey BW, Zolgharnain S. J. Vac. Sci. Technol., B. 1996; 14:3774–3781.
175. Chen Y, Pepin A. Electrophoresis. 2001; 22:187–207. [PubMed: 11288885]
176. Clough RL. Nucl. Instrum. Methods Phys. Res., Sect. B. 2001; 185:8–33.
177. Juang JY, Bogy DB. Microsyst. Technol. 2005; 11:950–957.
178. Marrian CRK, Tennant DM. J. Vac. Sci. Technol., A. 2003; 21:S207–S215.
179. McCord MA. J. Vac. Sci. Technol., B. 1997; 15:2125–2129.
180. Melngailis J. Nucl. Instrum. Methods Phys. Res., Sect. B. 1993; 80–81:1271–1280.
181. Wouters D, Schubert US. Angew. Chem. 2004; 43:2480–2495. [PubMed: 15127433]
182. Kochumalayil JJ, Meiser A, Soldera F, Possart W. Surf. Interface Anal. 2009; 41:412–420.
183. Pialat E, Trigaud T, Bernical V, Moliton JP. Mater. Sci. Eng., C. 2005; 25:618–624.
184. Reisner W, Beech JP, Larsen NB, Flyvbjerg H, Kristensen A, Tegenfeldt JO. Phys. Rev. Lett. 2007; 99:058302. [PubMed: 17930801]
185. Bilenberg B, Hansen M, Johansen D, Ozkapici V, Jeppesen C, Szabo P, Obieta IM, Arroyo O, Tegenfeldt JO, Kristensen A. J. Vac. Sci. Technol., B. 2005; 23:2944–2949.
186. Mahabadi KA, Rodriguez I, Haur SC, van Kan JA, Bettiol AA, Watt F. J. Micromech. Microeng. 2006; 16:1170–1180.
187. Wang LP, Shao PG, van Kan JA, Ansari K, Bettiol AA, Pan XT, Wohland T, Watt F. Nucl. Instrum. Methods Phys. Res., Sect. B. 2007; 260:450–454.
188. Shao PE, van Kan A, Ansari K, Bettiol AA, Watt F. Appl. Phys. Lett. 2006; 88:093515.
189. Yamasaki K, Juodkazis S, Matsuo S, Misawa H. Appl. Phys. A. 2003; 77:371–373.
190. Guo LJ, Cheng X, Chou CF. Nano Lett. 2004; 4:69–73.
191. Abgrall P, Low L-N, Nguyen N-T. Lab Chip. 2007; 7:520–522. [PubMed: 17389971]
192. Perry JL, Kandlikar SG. Microfluid. Nanofluid. 2006; 2:185–193.
193. Studer V, Pepin A, Chen Y. Appl. Phys. Lett. 2002; 80:3614–3616.
194. Zhang L, Gu F, Tong L, Yin X. Microfluid. Nanofluid. 2008; 5:727–732.
195. Dumond JJ, Low HY, Rodriguez I. Nanotechnology. 2006; 17:1975–1980.
196. Wu, J.; Chantiwas, R.; Soper, SA.; Park, S. Proceedings of International Mechanical Engineering Congress & Exposition (IMECE); Vancouver, British Columbia, Canada. 2010;

197. Gates BD, Xu Q, Stewart M, Ryan D, Willson CG, Whitesides GM. Chem. Rev. 2005; 105:1171–1196. [PubMed: 15826012]
198. Zaumseil J, Meitl MA, Hsu JWP, Acharya BR, Baldwin KW, Loo YL, Rogers JA. Nano Lett. 2003; 3:1223–1227.
199. Chen J-M, Liao S-W, Tsai Y-C. Synth. Met. 2005; 155:11–17.
200. Ionescu RE, Marks RS, Gheber LA. Nano Lett. 2005; 5:821–827. [PubMed: 15884878]
201. Tsai Y-C, Ho C-L, Liao S-W. Electrochem. Commun. 2009; 11:1316–1319.
202. Xie XN, Chung HJ, Sow CH, Wee ATS. Mater. Sci. Eng., R. 2006; 54:1–48.
203. Eijkel JCT, Bomer J, Tas NR, Berg A. v. d. Lab Chip. 2004; 4:161–163. [PubMed: 15159770]
204. Sivanesan P, Okamoto K, English D, Lee CS, DeVoe DL. Anal. Chem. 2005; 77:2252–2258. [PubMed: 15801761]
205. Cho YH, Park J, Park H, Cheng X, Kim BJ, Han A. Microfluid. Nanofluid. 2010; 9:163–170.
206. Faruqui D, Sharma A. Ind. Eng. Chem. Res. 2008; 47:6374–6378.
207. Muller-Buschbaum P, Bauer E, Maurer E, Schlogl K, Roth SV, Gehrke R. Appl. Phys. Lett. 2006; 88:083114.
208. Kim SO, Solak HH, Stoykovich MP, Ferrier NJ, de Pablo JJ, Nealey PF. Nature. 2003; 424:411–414. [PubMed: 12879065]
209. Kyrylyuk AV, Zvelindovsky AV, Sevink GJA, Fraaije J. Macromolecules. 2002; 35:1473–1476.
210. Tang CB, Tracz A, Kruk M, Zhang R, Smilgies DM, Matyjaszewski K, Kowalewski T. J. Am. Chem. Soc. 2005; 127:6918–6919. [PubMed: 15884912]
211. Xu T, Goldbach JT, Russell TP. Macromolecules. 2003; 36:7296–7300.
212. Xu B, Xu J, Xia X, Chen H. Lab Chip. 2010; 10:2894–2901. [PubMed: 20922216]
213. Wang Y, Liang XG, Liang YX, Chou SY. Nano Lett. 2008; 8:1986–1990. [PubMed: 18540656]
214. Shadpour H, Musyimi H, Chen J, Soper SA. J. Chromatogr., A. 2006; 1111:238–251. [PubMed: 16569584]
215. Kirby BJ, Hasselbrink Jr EF. Electrophoresis. 2004; 25:187–202. [PubMed: 14743473]
216. Kirby BJ, Hasselbrink Jr EF. Electrophoresis. 2004; 25:203–213. [PubMed: 14743474]
217. Schoch RB, Han J, Renaud P. Rev. Mod. Phys. 2008; 80:839.
218. Chai J, Lu F, Li B, Kwok DY. Langmuir. 2004; 20:10919–10927. [PubMed: 15568841]
219. Tandon V, Bhagavatula SK, Kirby BJ. Electrophoresis. 2009; 30:2656–2667. [PubMed: 19637218]
220. Jeong HE, Kim P, Kwak MK, Seo CH, Suh KY. Small. 2007; 3:778–782. [PubMed: 17352432]
221. Michalet X, Ekong R, Fougerousse F, Rousseaux S, Schurra C, Hornigold N, van Slegtenhorst M, Wolfe J, Povey S, Beckman JS, Bensimon A. Science. 1997; 277:1518–1523. [PubMed: 9278517]
222. Chan EY, Goncalves NM, Haeusler RA, Hatch AJ, Larson JW, Maletta AM, Yantz GR, Carstea ED, Fuchs M, Wong GG, Gullans SR, Gilmanshin R. Genome Res. 2010; 14:1137–1146. [PubMed: 15173119]
223. Neely RK, Dedecker P, Hotta J.-i. Urbanaviciute G, Klimasauskas S, Hofkens J. Chem. Sci. 2010; 1:453–460.
224. Douville N, Huh D, Takayama S. Anal. Bioanal. Chem. 2008; 391:2395–2409. [PubMed: 18340435]
225. Mannion J, Reccius C, Cross J, Craighead H. Biophys. J. 2006; 90:4538–4545. [PubMed: 16732056]
226. Li W, Tegenfeldt J, Chen L, Austin R, Chou S, Kohl P, Krotine J, Sturm J. Nanotechnology. 2003; 14:578–583.
227. de Gennes, PG., editor. Scaling Concepts in Polymer Physics. Cornell University Press; Ithaca, NY: 1979.
228. Odijk T. Macromolecules. 1983; 16:1340–1344.
229. Burgi DS, Chien RL. Anal. Chem. 1991; 63:2042–2047.

230. Gong M, Wehmeyer KR, Limbach PA, Arias F, Heineman WR. Anal. Chem. 2006; 78:3730–3737. [PubMed: 16737230]
231. Righetti PG, Bossi A. Anal. Chim. Acta. 1998; 372:1–19.
232. Koegler WS, Ivory CF. J. Chromatogr., A. 1996; 726:229–236.
233. Ross D, Locascio LE. Anal. Chem. 2002; 74:2556–2564. [PubMed: 12069237]
234. Chen L, Prest JE, Fielden PR, Goddard NJ, Manz A, Day PJR. Lab Chip. 2006; 6:474–487. [PubMed: 16572209]
235. Astorga-Wells J, Swerdlow H. Anal. Chem. 2003; 75:5207–5212. [PubMed: 14708796]
236. Lee JH, Song Y-A, Han J. Lab Chip. 2008; 8:596–601. [PubMed: 18369515]
237. Kim SM, Burns MA, Hasselbrink EF. Anal. Chem. 2006; 78:4779–4785. [PubMed: 16841895]
238. Lee JH, Chung S, Kim SJ, Han J. Anal. Chem. 2007; 79:6868–6873. [PubMed: 17628080]
239. Kim SJ, Han J. Anal. Chem. 2008; 80:3507–3511. [PubMed: 18380489]
240. Lee JH, Cosgrove BD, Lauffenburger DA, Han J. J. Am. Chem. Soc. 2009; 131:10340–10341. [PubMed: 19722608]
241. Cheow LF, Ko SH, Kim SJ, Kang KH, Han J. Anal. Chem. 2010; 82:3383–3388. [PubMed: 20307052]
242. Pennathur S, Santiago JG. Anal. Chem. 2005; 77:6772–6781. [PubMed: 16255573]
243. Baldessari F, Santiago J. J. Nanobiotechnol. 2006; 4:12.
244. Yuan Z, Garcia AL, Lopez GP, Petsev DN. Electrophoresis. 2007; 28:595–610. [PubMed: 17304495]
245. Pennathur S, Santiago JG. Anal. Chem. 2005; 77:6782–6789. [PubMed: 16255574]
246. Ajdari A, Bontoux N, Stone HA. Anal. Chem. 2006; 78:387–392. [PubMed: 16408918]
247. Garcia AL, Ista LK, Petsev DN, O'Brien MJ, Bisong P, Mammoli AA, Brueck SRJ, Lopez GP. Lab Chip. 2005; 5:1271–1276. [PubMed: 16234951]
248. Griffiths SK, Nilson RH. Anal. Chem. 2006; 78:8134–8141. [PubMed: 17134150]
249. Kato M, Inaba M, Tsukahara T, Mawatari K, Hibara A, Kitamori T. Anal. Chem. 2009; 82:543–547. [PubMed: 20030332]
250. Hao HY, Cremer Tinglu, Paul S. Anal. Chem. 2002; 74:379–385. [PubMed: 11811412]
251. Zhan W, Seong GH, Crooks RM. Anal. Chem. 2002; 74:4647–4652. [PubMed: 12349966]
252. Laurell T, Drott J, Rosengren L, Lindstrom K. Sens. Actuators, B. 1996; 31:161–166.
253. Letant SE, Hart BR, Kane SR, Hadi MZ, Shields SJ, Reynolds JG. Adv. Mater. 2004; 16:689–+.
254. Manjon A, Obon JM, Casanova P, Fernandez VM, Ilborra JL. Biotechnol. Lett. 2002; 24:1227–1232.
255. Chen G, McCandless GT, McCarley RL, Soper SA. Lab Chip. 2007; 7:1424–1427. [PubMed: 17960266]
256. Chen GF, McCarley RL, Soper SA, Situma C, Bolivar JG. Chem. Mater. 2007; 19:3855–3857.
257. Seok C, Jeong Hoon L, Myoung-Woon M, Jongyoon H, Roger DK. Adv. Mater. 2008; 20:3011–3016.

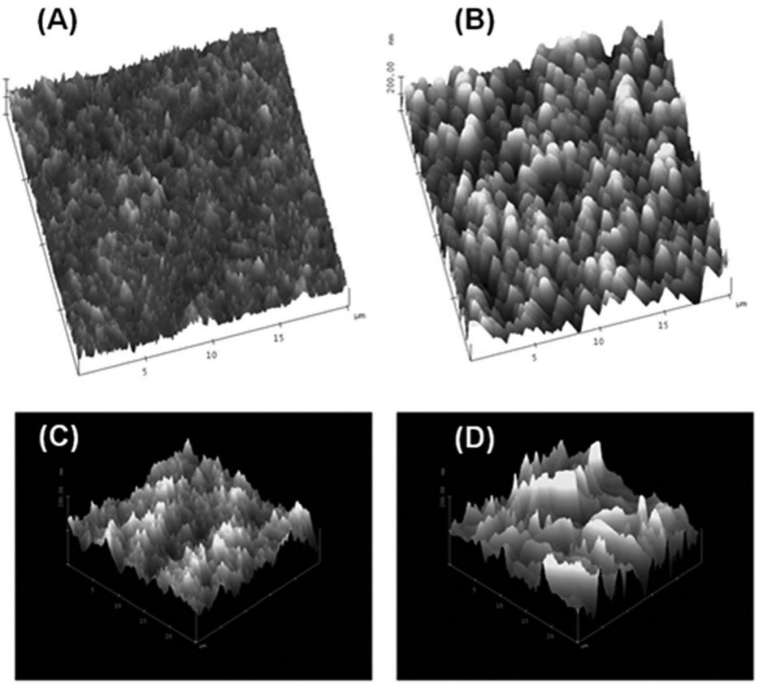

Fig. 1.

Tapping mode AFM images of PMMA that has been treated with either UV radiation or an oxygen plasma showing the effects of the treatment on the surface roughness. (A) Native PMMA with an RMS roughness of 18 nm. (B) The same PMMA surface as in (A), but treated with UV radiation for 30 s; RMS roughness was found to be 27.5 nm. (C) Another PMMA surface (native) interrogated using tapping mode AFM with an RMS roughness of 16.7 nm. (D) Same PMMA surface as in (C), but plasma treated at 500 mW for 2 min and possessing an RMS roughness of 28.6 nm. The micrographs were reproduced with permission from Wei *et al.* (2005)[62] and Xu *et al.* (2007).[49]

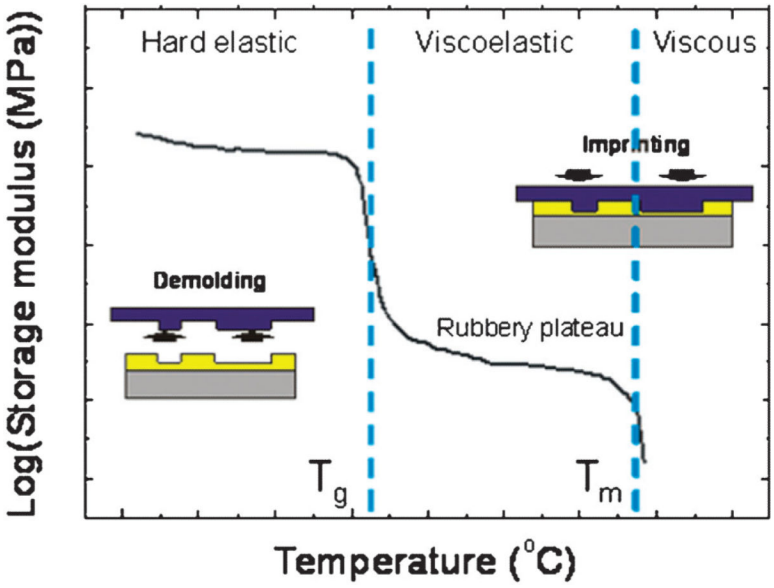

Fig. 2.

Typical behavior of the storage modulus for thermoplastic polymers that is dependent on the temperature. T_g and T_m represent the glass transition temperature and melting temperature, respectively. NIL or hot embossing is usually performed above the T_g either in the viscoelastic or viscous state while demolding is done in the hard glassy state below the T_g.

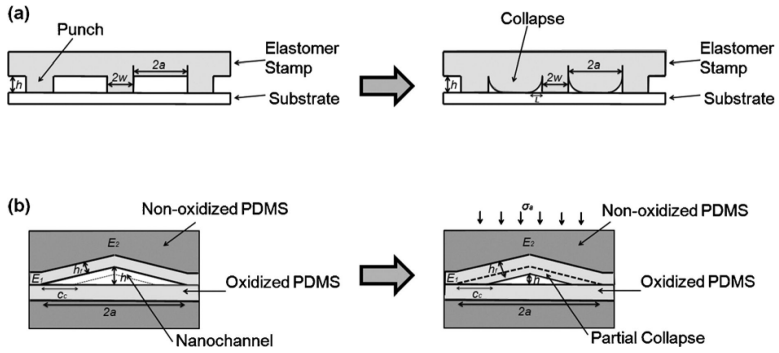

Fig. 3.

Schematic showing the collapse of elastomeric channels; (a) roof collapse (b) collapse of crack induced-triangular nanochannels.

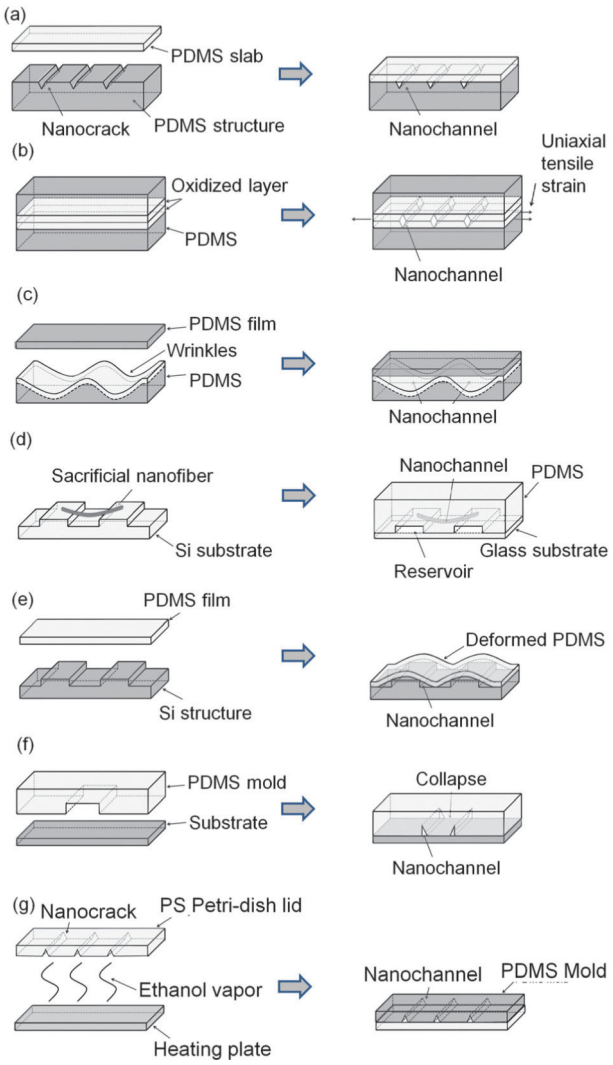

Fig. 4.

Schemes for nanoslit and nanochannel fabrication in PDMS. Fabrication of crack-induced (a) normally-open nanochannels; (b) normally-closed nanochannels. (c) Fabrication of nanochannels using wrinkles made by surface buckling. (d) Nanochannel fabrication using sacrificial electrospun nanofibers. (e) Fabrication of nanochannels by deformation of a thin layer of PDMS over nanotopography. (f) Nanochannel fabrication by collapse of micron-scale PDMS microchannels. (g) Nanochannel fabrication with PS Petri-dish cracking.

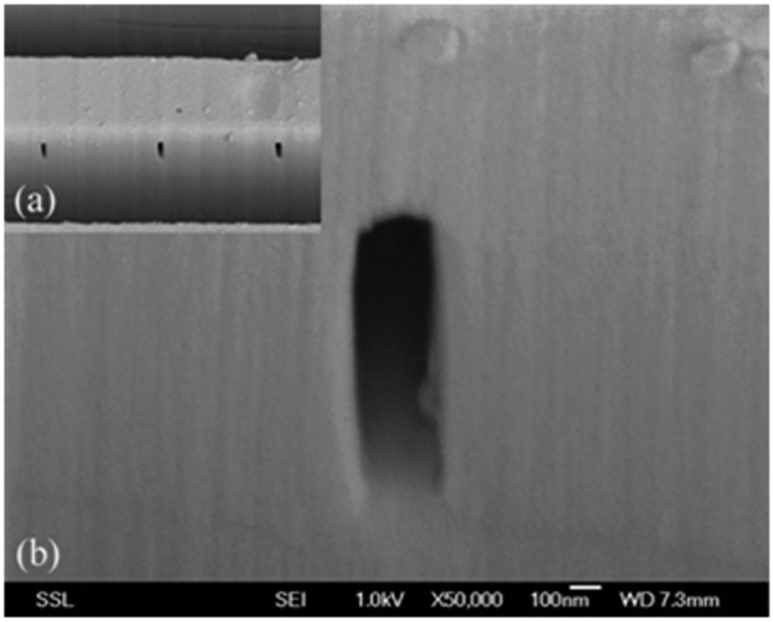

Fig. 5.

(a) PMMA enclosed nanochannels fabricated using proton beam writing coupled with thermal bonding, and (b) high magnification view of one of the buried channels. The channels are 200 nm wide and 2 μm deep. The proton beam was a 2 MeV energy beam that consisted of a 200 × 300 nm^2 spot size and was scanned over a 2 μm thick layer of PMMA layer spin coated onto a 50 μm Kapton film. Reprinted with permission from Shao *et al.* (2006).[188]

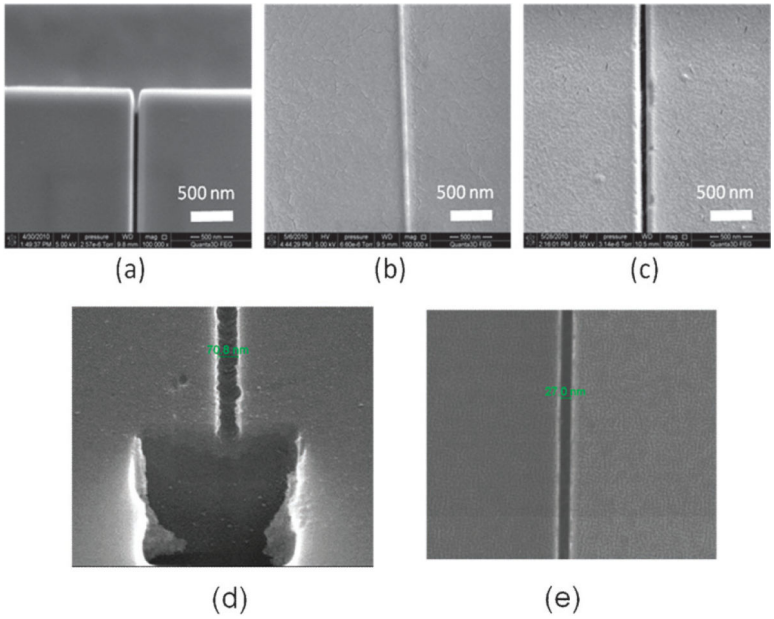

Fig. 6.

SEMs of a 60 nm channel produced in (a) a Si master, (b) UV curable polymer stamp replicated from the Si master, and (c) imprinted PMMA produced using the polymer stamp shown in (b). The nanochannel shown in (a) was made by FIB milling using a Ga^+ ion beam into a Si ⟨100⟩ substrate. A monolayer of 1H, 1H, 2H, 2H-perfluoro-decyltrichlorosilane was coated onto the patterned substrate. To create the polymer stamp, a UV-curable polymeric blend containing 69 wt% tripropylene glycol diacrylate (TPGDA) as the base, 29 wt% trimethylol-propane triacrylate as the crosslinking agent, and 2 wt% Irgacure 651 as the photo-initiator were used. The Si master was coated with the UV resin by dispensing with a pipette. Then, a COC substrate (COC-TOPAS 6017, TOPAS Advanced Polymers, Florence, KY) was placed on the UV resin-coated stamp and was gently pressed in order to ensure complete filling of the resin into the master cavities. This was followed by UV exposure for 20 s to allow for curing. The UV lamp used for curing had an intensity of 1.8 W cm^{-2}. The patterned UV-curable resin was then used as a stamp to hot impress into a 3 mm-thick PMMA sheet. The imprinting was carried out at 130 °C and 20 bars for 5 min using an NIL machine (Obducat nanoimprint system), with an applied pressure to the stamp and substrate using compressed air, ensuring pressure uniformity over the entire imprint area. The pressure was added after a 30 s preheating at the desired molding temperature and was kept constant during the imprinting process until cooled to 70 °C. After the stamp and substrate were cooled to room temperature, the PMMA replica was removed from the UV-resin stamp. (d), (e) SEMs showing 71 nm and 27 nm channels, respectively, fabricated directly in a quartz substrate using FIB milling (Ga^+ ion beam). In all cases, the channels shown were not sealed with a cover plate. For (d), the FIB was used to cut a cross-section from the substrate following nanochannel patterning to inspect the topology of the channel. In all cases, the aspect ratio of the channels shown in this figure were ~1 (aspect ratio = channel depth/channel width).

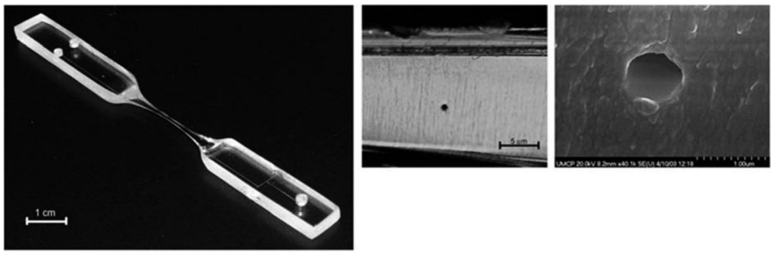

Fig. 7.

(a) Typical fabricated nanofluidic chip *via* thermomechanical deformation of a thermoplastic, in this case PC. (b) Far-field and (c) high magnification electron micrographs showing a single nanochannel with a circular cross section of 700 nm in diameter. PC pre-forms, consisting of microchannels, were placed between two Ni–Cr resistive radiant heaters and heated above the T_g of the polymer; linear motors were used to pull the microchannel to the desired nm diameter. This technique could be used to form nanochannels with diameters up to 400 nm. Reprinted with permission from Sivanesan *et al.* (2005).[204]

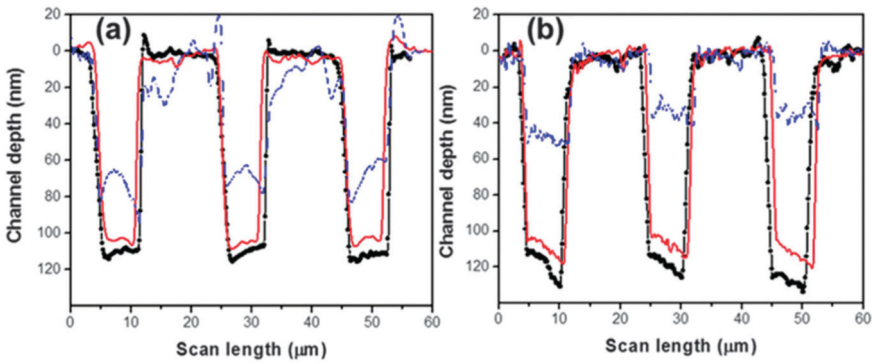

Fig. 8.

AFM profiles measured for (a) PMMA and (b) COC nanoslits (7 μm wide, ~100 nm deep, 12 μm pitch) before and after different cover plate assembly protocols. The blue-dash line represents the slit depth following thermal fusion bonding at 107 °C for PMMA and at 130 °C for COC slits; red-solid line is the depth of the slits following thermal fusion bonding at 87 °C and 115 °C of an oxygen plasma treated substrate and cover plate for PMMA and COC, respectively; and the black-circle line is the nanoslits following molding, but not subjected to thermal fusion bonding. Reprinted with permission from Chantiwas *et al.* (2010).[59]

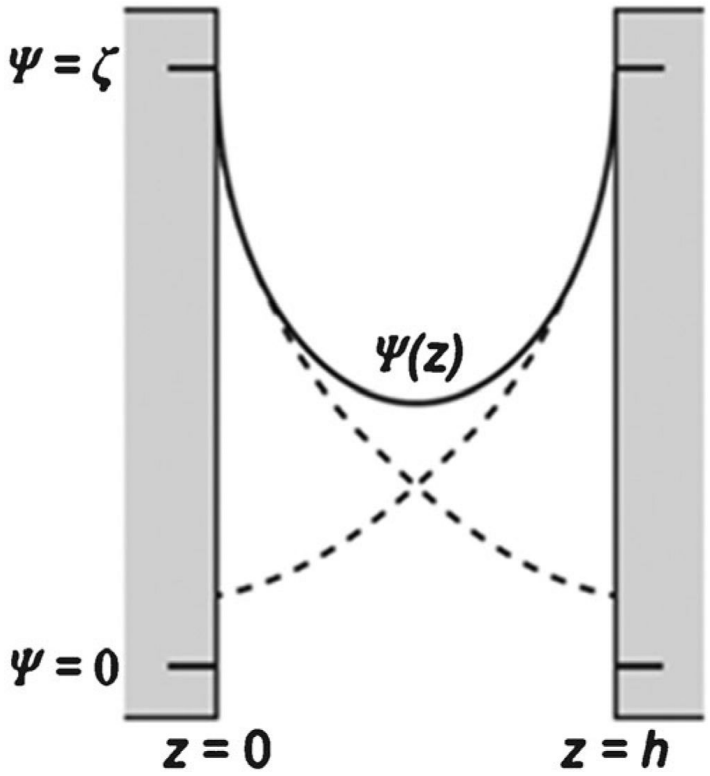

Fig. 9.

Schematic representation of the potential distribution in a nanochannel with height *h* in direction *z* when the EDLs overlap (solid line), compared to the EDL potentials if the opposite wall is not present (dashed line). Reproduced with permission from Schoch *et al.* (2006).[217]

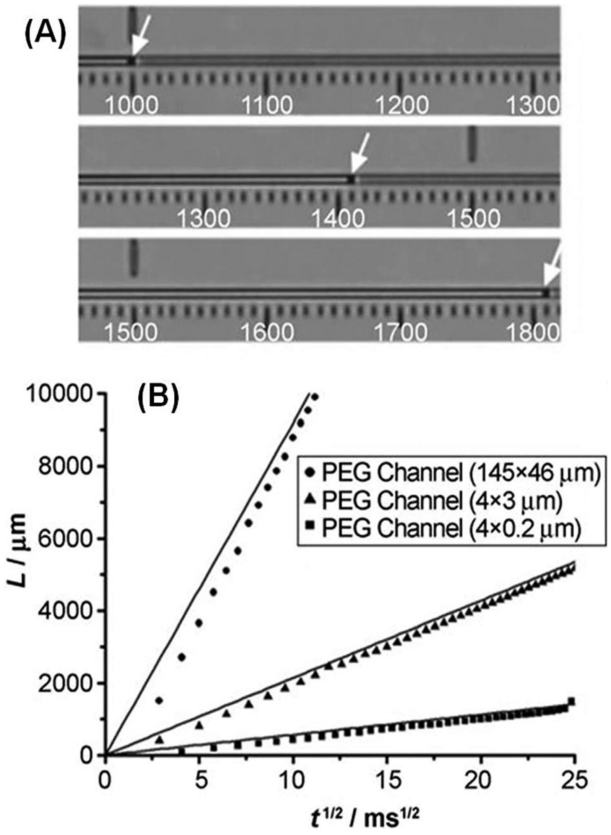

Fig. 10.

Capillary flow in PEG microchannels and a PEG nanoslit. (A) Optical micrograph showing the movement of water through a PEG channel *via* capillary pressure. (B) A plot of the water front position, *L*, *versus* $t^{1/2}$. As can be seen from the data, for the 4 μm × 200 nm nanoslit, the experimental data followed that predicated by Poiseuille flow, even for small rectangular channels (R = 0.19 μm). For these PEG rectangular slits, the water contact angle was found to be 53°. Reproduced with permission from Jeong *et al.* (2007).[220]

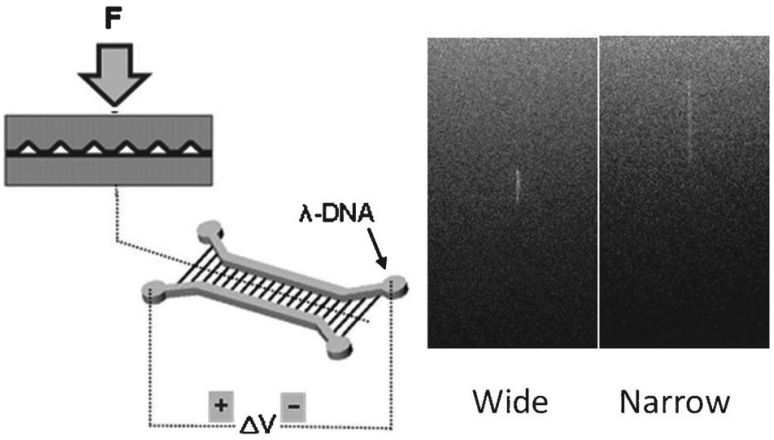

Fig. 11.

Dynamic modulation of DNA linearization in PDMS nanoslits through reduction of the cross-sectional area by application of an external force. The left schematic represents the concept of applying an external force to partially collapse the triangular cross section nanoslits that bridge two microchannels. Shown on the right are micrographs of the same λ-DNA molecule linearized to different degrees depending on whether the cross sectional area is wide or narrow. The DNA molecule was linearized to ~6 μm in the wide state and ~14 μm in the narrow state. Adapted with permission from Huh *et al.* (2007).[165]

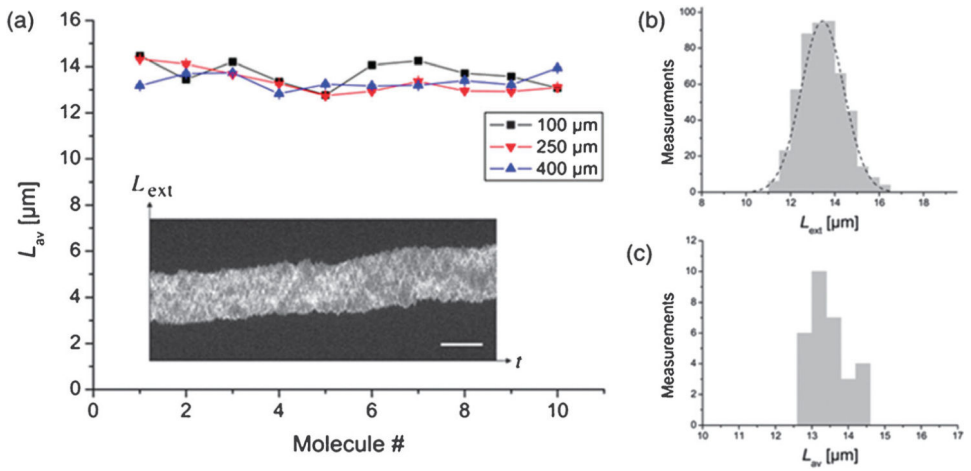

Fig. 12.

(a) Graphs showing the average extension length L_{av} of 10 different T4 DNA molecules inside a PMMA nanochannel. L_{av} was measured 100, 250 and 400 μm from the nanochannel entrance for each molecule. The inset shows a typical intensity time-trace of a T4 molecule confined inside the PMMA nanochannel. The scale bar is 10 μm and the time span is 50 s. (b) Histogram of the measured extension lengths L_{ext} of DNA molecule 2 positioned 100 μm from the nanochannel entrance. The average extension, L_{av}, was found to be 13.4 μm and the standard deviation σ_{av} = 1.0 μm. The dashed line shows the Gaussian curve fit. (c) Histogram of the measured L_{av} presented in (a). The overall average extension length was 13.5 μm with a standard deviation of 0.5 μm. The PMMA nanofluidic device was made *via* NIL using a hybrid stamp (micro- and nanostructures). The nanochannel possessed dimensions of 250 × 250 nm. Reproduced with permission from Thamdrup *et al.* (2008).[159]

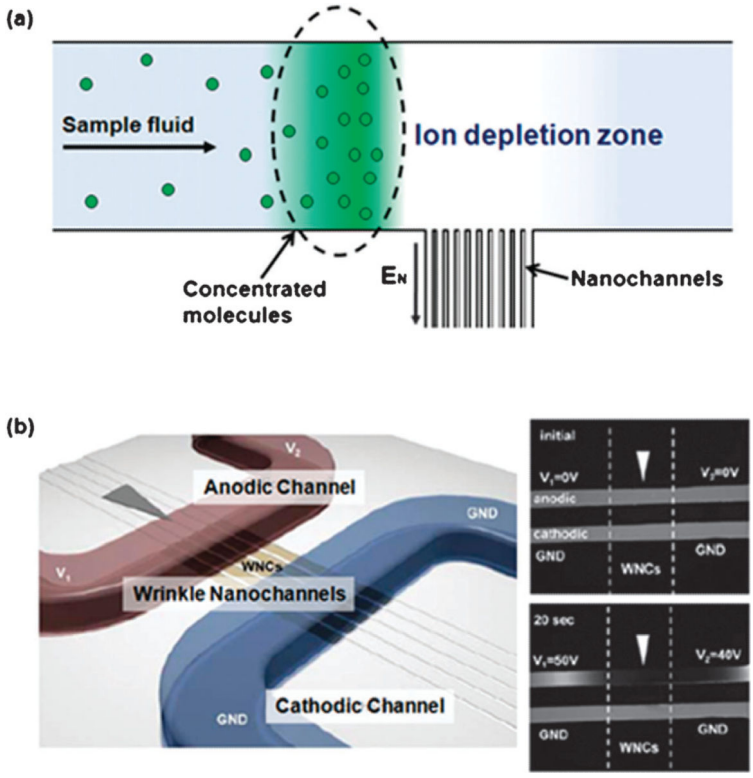

Fig. 13.

Molecular preconcentration in a nanofluidic system. (a) Mechanism of molecular preconcentration by ion depletion in the vicinity of the nanochannel. (b) Preconcentration of β-phycoerythrin using a PDMS wrinkle nanochannel device. Reproduced with permission from Chung *et al.* (2008).[169]

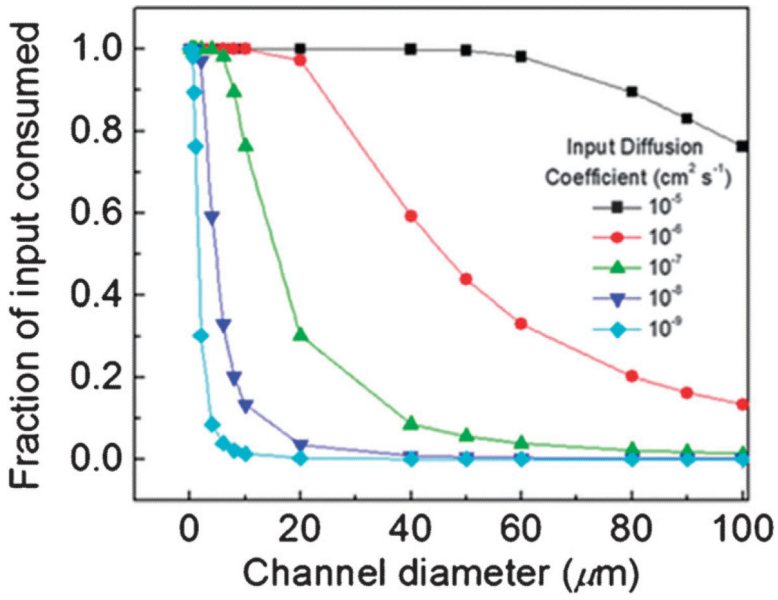

Fig. 14.

Relative amount of input target converted as a result of a solid-phase enzymatic reaction for a hypothetical molecule with given diffusion coefficient, D_A, traveling through a reactor of various dimensions. The response was modeled using the equation shown in Section 4.4. The values used for calculating the conversion were $l = 1.0$ cm; $\nu = 1.0$ cm s^{-1}.

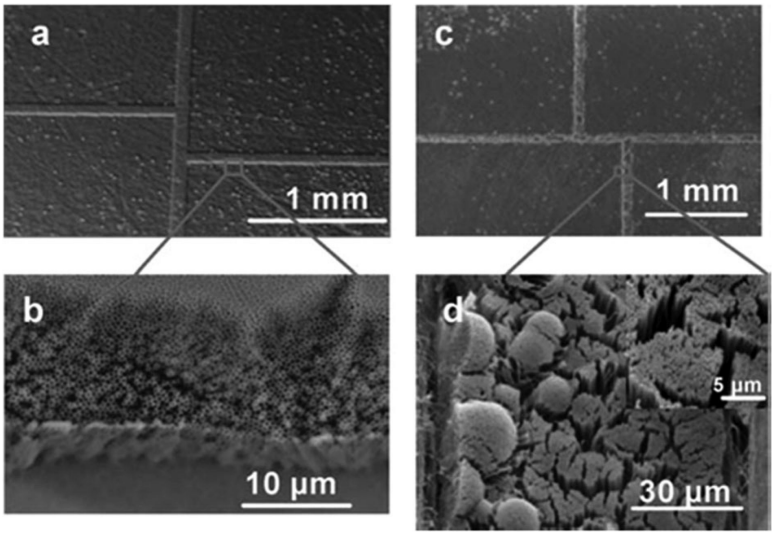

Fig. 15.

SEM images of the AAO/Al template prepared by UV lithography (a), (c) and the corresponding microstructures containing nanopillars (b), (d). In (a) and (c) are shown 'double T' fluidic channels (50 μm wide, 100 μm deep); (b) side view of the AAO micromold populated with nanopores (150 nm in diameter and 100 μm in height); (d) a top view of the molded microchannel filled with nanopillars (150 nm diameter and 100 μm height). The fluidic structures were made *via* high precision micromilling of an AAO template, followed by pre-polymer injection over the AAO template, polymerization, Al removal, thermal fusion bonding of a polymer cover plate and removal of the AAO template. Reproduced with permission from Chen *et al.* (2006).[255]

Table 1

Common polymers and their physiochemical properties and comparison to glass

Material	Acronym	T_g/°C	T_m/°C	CTE (α) ppm °C^{-1}	Refractive index	Young's modulus/GPa	Optical transmissivity	
							UV	Vis
Polystyrene	PS	92–100	240–260	10–150	1.55–1.59	3.3–3.5	Poor	Excellent
Polycarbonate	PC	145–148	260–270	60–70	1.584	2.0–2.4	Poor	Excellent
Poly(methyl methacrylate)	PMMA	100–122	250–260	70–150	1.492	1.8–3.1	Good	Excellent
Cyclic olefin co(polymer)	COC	70–155	190–320	60–80	1.53	2.6–3.2	Excellent	Excellent
Poly(ethylene terephthalate)	PET	69–78	248–260	48–78	1.575	2.0–2.7	Good	Good
Polypropylene	PP	–20	160	18–185	1.49	1.5–2.0	Fair	Good
Poly(dimethylsiloxane)	PDMS	–125	–55	67.3	1.40	$0.36–0.87 \times 10^{-3}$	Excellent	Excellent
Glass (Soda lime)	G	520–600	1040	9	1.52	50–90	Good	Excellent

CTE—Coefficient of thermal expansion (linear).

Table 2

Nanochannels/nanoslits fabricated in various polymeric materials along with the characteristic geometry of the structures and their reported application

Material	Dimension (nm, width × depth)	Fabrication method	Application	Reference
PDMS	690 × 80	Crack-induced tunable	λDNA stretching	Huh *et al.* (2007)[165]
PDMS	7×10^3 nm^2 (area)	Tunnel cracking	Nanoparticle trapping	Mills *et al.* (2010)[166]
PDMS	1470 × 275	Wrinkle induced by oxygen plasma	Protein preconcentration	Seok *et al.* (2008)[257]
PDMS	100, 500 (depth)	Deformation of thin PDMS	DNA stretching	Park *et al.* (2009)[171]
PDMS	200 × 60	Collapse of micron-scale PDMS microchannels. Glass/PDMS bonding substrate	DNA elongation and surface enhanced Raman detection of nucleic acids	Park *et al.* (2009)[172]
PDMS	400 × 20	Nanochannels cracked from PS petri-dish induced by ethanol	Ion selective enrichment	Xu *et al.* (2010)[37]
PMMA	200 × 2000	Proton beam writing, thermal fusion bonding	NA	Shao *et al.* (2006)[188]
SU-8, SiO_2 layer	250 × 250	EBL and NIL, thermal fusion bonding	DNA stretching	Thamdrup *et al.* (2008)[159]
PMMA, COC, PC	3000/7000 × 100	Nanomolding replication, NIL, oxygen plasma treatment with thermal fusion bonding	λDNA transport dynamics and DNA mobilities	Chantiwas *et al.* (2010)[59]
PMMA	300 × 500, 300 × 140 and 75 × 120	Imprinting nanostructure from Si etched into PMMA thin film	DNA stretching	Guo (2004)[134]
PMMA	10 000 × 80	Si molding with thermal fusion bonding	NA	Abgrall *et al.* (2007)[191]
PC	100-900 wide, 200 nm wire	Hot embossing of silica nanowire molding with PC substrate, PDMS for cover plate bonded material	NA	Zhang *et al.* (2008)[194]
PMMA	185 × 85	Replication of polymer stamp and polymer nanofluidic channels by NIL using polymer stamp	NA	Wu *et al.* (2010)[196]
PI (Polyimide)	2000-30 000 wide, 100 and 500 nm deep	Spin coat PI onto Si wafer and deposition of Al as sacrificial layer; etch Al, deposit another layer of PI and remove patterned Al	EOF measurements	Eijkel *et al.* (2004)[203]

Table 3

Experimental values of ζ and σ for untreated and 50 s oxygen plasma treated PMMA in different electrolyte solutions. Data taken with permission from Chai *et al.* (2004)[218]

Sample	Solution	ζ/mV	σ/μC cm^{-2}
No treatment	Water	–35.9	–0.0089
	0.1 mM KCl	–13.4	–0.031
	1 mM KCl	–7.5	–0.055
50 s treatment	Water	–82.5	–0.028
	0.1 mM KCl	–48.5	–0.130
	1 mM KCl	–20.9	–0.157